The Usefulness of In-Flight Measurements of Space Count to Improve Calibration of the AVHRR Solar Reflectance Bands

ALEXANDER IGNATOV, CHANGYONG CAO, AND JERRY SULLIVAN

NOAA/NESDIS/Office of Research and Applications, Camp Springs, Maryland

ROBERT LEVIN

NOAA/NESDIS/Office of Satellite Data Processing and Distribution, Suitland, Maryland

XIANGQIAN WU

NOAA/NESDIS/Office of Research and Applications, Camp Springs, Maryland

ROY GALVIN

ITT Aerospace/Communications, Radiometric Products Group, Fort Wayne, Indiana

(Manuscript received 20 April 2004, in final form 23 July 2004)

ABSTRACT

The solar reflectance bands (SRB; centered at $\lambda_1 = 0.63$, $\lambda_2 = 0.83$, and $\lambda_{3A} = 1.61$ μm) of the Advanced Very High Resolution Radiometers (AVHRR) flown on board NOAA satellites are often referred to as noncalibrated in-flight. In contrast, the Earth emission bands (EEBs; centered at $\lambda_{3B} = 3.7$, $\lambda_4 = 11$, and $\lambda_5 = 12$ μm) are calibrated using two reference points: deep space and the internal calibration targets. In the SRBs, measurements of space count (SC) are also available; however, historically they are not used to specify the calibration offset [zero count (ZC)], which does not even appear in the calibration equation. A regression calibration formulation is used instead, equivalent to setting the ZC to a constant, whose value is specified from prelaunch measurements.

The analyses below, supported by a review of the instrument design and a wealth of historical SC information, show that the SC varies in-flight and differs from its prelaunch value. It is therefore suggested that 1) the AVHRR calibration equation in the SRBs be reformulated to explicitly use the ZC, consistently with the EEBs; and 2) the value of ZC be specified from the onboard measurements of SC. The ZC formulation of the calibration equation is physically solid, and it minimizes human-induced calibration errors resulting from the use of a regression formulation with an unconstrained intercept. Specifying the calibration offset improves radiances, most notably at the low end of radiometric scale, and subsequently provides for more accurate vicarious determinations of the calibration slope (gain). These calibration improvements are important for the products derived from the AVHRR low radiances, such as aerosol over ocean, and are particularly critical when generating their long-term climate data records (CDRs).

1. Introduction

Three generations of the Advanced Very High Resolution Radiometers (AVHRR) have been flown on board the National Oceanic and Atmospheric Administration (NOAA) platforms since 1978 (e.g., Cracknell 1997). The AVHRR/3 will be flown on board the two future NOAA platforms N and N′ scheduled for launch in 2005 and 2008, and three METOP platforms 1–3 planned for launch in 2005, 2010, and 2014, respectively. Thus the AVHRR data record is expected to continue through at least 2020. Ensuring accurate and consistent calibration of all AVHRR sensors is essential for creating high quality products, and especially generating their long-term climate data records (CDRs) that would eventually span over 40 yr of data.

The AVHRR carries two types of bands: the solar reflectance bands (SRBs) that measure solar radiation reflected from Earth's surface and atmosphere to space, and the Earth emission bands (EEBs) that measure radiation originating from the Earth emission itself. The space count (SC) is measured in all bands, and yet it is used to specify the "zero count" (ZC) in the calibration equation for the EEBs only. This study

Corresponding author address: Dr. Alex Ignatov, E/RA3, Rm. 603, 5200 Auth Rd., Camp Springs, MD 20746-4304.
E-mail: alex.ignatov@noaa.gov

seeks to evaluate the potential use of the SC data to improve the current operational AVHRR calibration in the SRBs. The analyses are based on careful examination of the instrument design and extensive data analyses. Our conclusions reiterate and elaborate on the two points made elsewhere that the physically based ZC formulation [calibration Eq. (3) below] is preferred over the current regression formulation [Eq. (4) below; cf. Weinreb et al. 1997], and that the value of ZC in Eq. (3) should be specified from onboard SC measurements (cf. Mitchell 2001). Once implemented, these developments would significantly improve low radiances in the AVHRR SRBs and the quality of products derived therefrom, such as aerosol over ocean, and subsequently improve the vicarious determination of the calibration slope (gain).

The paper is organized as follows. In section 2, the two current calibration mechanisms used in the EEBs and SRBs are compared and shown to be inconsistent. The emphasis here is that the ZC parameter (which appears in the calibration equation) should be clearly distinguished from the measured SC (which is a measured quantity subject to data errors). The long-term nature of discarding the SC data in the SRBs (over 25 yr, since the AVHRR inception in 1978) requires careful and detailed review of the AVHRR SC measurements in section 3. Particular attention is paid to the so-called clamping mechanism, which is supposed to maintain the SC at a constant level (~40 count in the SRBs), and is the key to understanding the information potential of the AVHRR SC data. Section 4 gives a few examples of the Moon affecting the SC. These cases are rare and extreme for the AVHRR, and we suggest that the "contaminated" data should be excluded from the analyses. However, these data "anomalies" provide insight into the mechanism of the AVHRR clamping circuit. Also, they help quantify the effect of changes in the SC on the daytime Earth-view data, and clearly make the point that the real SC data should be utilized in the SRB calibration. Section 5 sets the stage for the long-term analyses in section 6 by presenting several examples of the "normal" (i.e., not-anomalous) SC orbital statistics for *NOAA-15* and *-16*. The effect of digitization in the SC data may lead to errors in estimating the ZC (cf. Mitchell 2001). Potential use of the "night counts" (i.e., Earth view on the dark side of orbit) to supplement the SC is also explored in section 5. Section 6 documents long-term time series of the SC orbital statistics for a number of NOAA platforms from 1994 to the present. The results are presented and discussed in a context of some past empirical prelaunch and in-flight SC analyses. Section 7 summarizes and concludes the paper.

2. AVHRR calibration background

The AVHRR/1 flown on *TIROS-N* and *NOAA-6*, *-8*, and *-10* had two SRBs centered at $\lambda_1 = 0.63$ and $\lambda_2 = 0.83$ μm (bands 1 and 2), and two EEBs at ~3.7 and ~11 μm (bands 3 and 4).[1] On AVHRR/2 flown on board *NOAA-7*, *-9*, *-11*, *-12*, and *-14*, a third EEB was employed centered at ~12 μm (band 5); and on AVHRR/3 flown on *NOAA-15*, *-16*, and *-17*, a new SRB was added at $\lambda_3 = 1.61$ μm and termed 3A to differentiate it from the former band 3 at 3.7 μm that is newly termed 3B. The 3A/3B bands are time-shared according to the "either/or" logic that is reprogrammable from Earth, so that data in one band or the other are always available, but never both together. By default, the switchover occurs at the terminator (Sun angle, $\theta_o = 90°$). Note that AVHRR/3 will be also employed on the two afternoon platforms, NOAA-N and N′ (to be launched in February 2005 and 2008, respectively), and three morning platforms, METOP 1–3 (to be launched in 2005, 2010, and 2014, respectively).

In the AVHRR, the Earth-view radiance[2] in band i is reflected by a rotating scan mirror toward the input optics, converted to a voltage by the view electronics, digitized, and transmitted to the ground as a 10-bit count (0–1023), C_{Ei}. On the ground, the Earth radiance is calculated from the measured count via a calibration procedure. Presently, the EEBs and SRBs are calibrated differently. In the two subsections below, the two calibration mechanisms are compared, with the objective to more clearly present the argument that more consistency should be sought between the two procedures.

a. Calibration of the AVHRR EEBs

In the EEBs, the Earth radiance L_{Ei} [W/(m^2 cm^{-1} sr)] is calculated from the 10-bit Earth count, C_{Ei}, as (e.g., Cracknell 1997)

$$L_{Ei} = G_i^{-1}(C_{Ei} - C_{oi}). \quad (1)$$

The "zero count," C_{oi}, corresponds to a zero input radiance ($L_{oi} = 0$), and the calibration gain G_i is calculated using a second reference point, with a reference count (RC) C_{ri} corresponding to a reference radiance, L_{ri}, as

$$G_i^{-1} = \frac{L_{ri} - L_{oi}}{C_{ri} - C_{oi}}. \quad (2)$$

In the NOAA operations, the interpolation is linear in count in band 3B, as Eqs. (1)–(2) suggest, whereas in

[1] On the sunlit part of the orbit, band 3 is also sensitive to reflected solar radiation, in addition to Earth emission. It is still considered an EEB here from the standpoint of its calibration (Trishchenko 2002).

[2] Note that the term "Earth-view radiance" (and the "E" subscript) are used throughout this paper to indicate the *scan position of the AVHRR mirror*, or the target at which the AVHRR is pointing [i.e., *Earth* ("E") as opposed to *space* ("S") and onboard *blackbody* ("B"); see section 3a for detail]. This should *not* be confused with the physical origin of the radiation [i.e., photons emitted by the Sun and reflected by Earth toward AVHRR (in the SRBs) versus those emitted by Earth itself (in the EEBs)].

bands 4 and 5, a nonlinearity correction is applied (Sullivan 1999; Goodrum et al. 2003). [Note that users of NOAA data usually convert radiances in the EEBs to the equivalent brightness temperatures (Kidwell 1998; Goodrum et al. 2003).]

In-flight, the ZC and RC are estimated from the space count (SC) C_{Si} and blackbody count (BC) C_{Bi}, respectively. At each scan line, 10 SCs and 10 BCs are recorded in each band, when the scan mirror points to deep space and the onboard blackbody [or internal calibration target (ICT)], respectively. The reference radiance, L_{ri}, is approximated with the Planck function at ICT temperature, L_{Bi} (T_B), which is measured in-flight by four platinum resistance thermometers (PRTs). A nominal target temperature is $T_B \sim 290$ K, but the actual T_B depends upon many factors and may be anywhere within a few kelvins of the target value.

We emphasize that the calibration parameters in Eqs. (1)–(2), C_{oi}/C_{ri} and L_{oi}/L_{ri}, should be clearly distinguished from their onboard-measured counterparts, C_{Si}/C_{Bi} and L_{Si}/L_{Bi} [actually, the two radiances are not measured on board, but rather assumed to be zero (L_{si}) and calculated from the PRT temperatures (L_{Bi}), respectively], which are subject to data errors (outliers, biases, and random errors from digitization and noise) and/or violation of calibration assumptions. Outliers and biases may result from glitches occurring during the data acquisition/transmission/reception (e.g., Trishchenko 2002), or from occasional contamination of the space/ICT views by the Moon or Sun (e.g., Cao et al. 2001, and analyses in section 4 below). Sharp anomalies (outliers) in the measured C_{Si}/C_{Bi} can be removed, for example, by a Fourier transform filtering (Trishchenko and Li 2001), and the noise/digitization suppressed by averaging/smoothing (e.g., Weinreb et al. 1997; Trishchenko 2002; Trishchenko et al. 2002). The deep-space radiance is assumed to be zero, and estimating L_{ri} from L_{Bi}, assumes that the ICT is a perfect blackbody and that the four PRTs onboard measure its true temperature error-free. These assumptions may be violated, too, and steps may be needed to correct for these effects (e.g., Trishchenko 2002; Trishchenko et al. 2002). Estimating the calibration parameters in Eqs. (1)–(2) should thus include some preprocessing/quality control of the onboard measurements to mitigate the data errors. The resulting C_{oi}/C_{ri} are not necessarily integer numbers, albeit they are estimated from the integer C_{Si}/C_{Bi}.

b. Calibration of the AVHRR SRBs

In the SRBs, the Earth-view radiance, L_{Ei} [W m^{-2} μm^{-1} sr^{-1}] could be derived from C_{Ei} via an analog of Eq. (1) (and we argue that this generic form of the calibration equation actually *should* be used):

$$L_{Ei} = G_i^{-1}(C_{Ei} - C_{oi}). \quad (3)$$

In-flight, the value of ZC can be specified from the SC (C_{Si}) that is measured in the SRBs, too, but the calibration slope (gain, G_i) cannot, because the second reference calibration point (radiance source or solar diffuser) is missing. This is why the AVHRR SRBs are often referred to as "noncalibrated onboard" (e.g., Cracknell 1997), which is, however, only half true, as was rightly pointed out by Mitchell (2001). To monitor gain in-flight via an analog of Eq. (2), a second reference target must thus be specified vicariously (e.g., Kaufman and Holben 1993; Teillet and Holben 1994; Rao and Chen 1995, 1999; Minnis et al. 2002; Tahnk and Coakley 2002). The determination of the calibration slope is obviously improved, if the intercept is specified more accurately.[3]

Note that in the NOAA operations, the radiance is converted to the Earth normalized reflectance (termed at NOAA the "overhead Sun albedo") defined as A_{Ei} (%) $= 100\,\pi L_{Ei}/F_i$, where F_i (W m^{-2} μm^{-1}) is the solar flux. (Note that this definition may be confusing to a user of NOAA data who is used to reflectances normalized by cosine of solar zenith angle, $\mu_o = \cos\theta_o$, as $\rho_{Ei} \equiv A_{Ei}/\mu_o$, but it is convenient for calibration purposes because it is just the scaled radiance.)

In the laboratory, the space measurement is imitated when AVHRR views the external space clamp target or the external calibrating sphere with all lamps off (e.g., Cracknell 1997). The resulting "SC" statistics (mean and STD) are reported in the respective ITT manuals, which show differences between the AVHRR instruments (e.g., ITT 1997, 1999, 2002). The space target data that are considered to be more reliable are summarized for different AVHRRs in Table 1a. The mean SC, C_{Si}, is typically within a few counts of ~40, which is a target number for all AVHRR SRBs (see section 3). The STD SC, σC_{Si}, quantifies the level of radiometric noise in a channel, a useful parameter to estimate the respective noise in the product (e.g., Ignatov 2002). In comparing the σC_{Si} for different instruments, one should keep in mind that on AVHRR/3, the digitization in the low gain was improved compared to AVHRR/1 and /2. As a result, one AVHRR/3 count is equivalent to approximately one-half of AVHRR/1 and /2 count in bands 1 and 2, and to approximately one-quarter in band 3A. Therefore, for cross-comparisons of the σC_{Si} in Tables 1a and 1b, data of Table 1b should be multiplied by roughly a factor of ~0.5 (bands 1 and 2) or ~0.25 (band 3A) to arrive at equivalent AVHRR/1/2 estimate. The scaled AVHRR/3 σC_{Si} are all in the range 0.05–0.20 count and tend to be lower compared to the respective AVHRR/1 and/2 estimates in Table 1a (from 0.05 to 0.50). At least a part of the AVHRR/3 improvement over its predecessors may be attributed to

[3] The AVHRR/3 uses different calibrations ("gains") for $C_i < 510$ and $C_i > 510$, whose respective parameters in the calibration Eq. (3), C_{oi} and G_i, differ. Estimating C_{oi} from C_{Si} is possible for the "low gain" but not for the "high gain." Detailed discussion of the high gain is beyond the scope of this study.

TABLE 1a. Preflight (laboratory) measurements of mean/STD SCs for AVHRR/1 and /2 according to ITT manuals.

Platform	Instrument	Band 1 (λ_2 = 0.63 μm)		Band 2 (λ_2 = 0.83 μm)	
		C_{S1}	σC_{S1}	C_{S2}	σC_{S2}
TIROS-N	AVHRR/1 (PFM)	37.55	0.49	39.56	0.48
NOAA-6	AVHRR/1 (A103)	37.97	0.20	40.00	0.08
NOAA-7	AVHRR/2 (A201)	37.56	0.47	39.58	0.48
NOAA-8	AVHRR/1 (A102)	40.00	0.04	42.99	0.08
NOAA-9	AVHRR/2 (A202)	38.77	0.33	40.05	0.30
NOAA-10	AVHRR/1 (A101)	36.05	0.32	37.88	0.47
*NOAA-11**	AVHRR/2 (A203)	40.83	0.36	40.42	0.48
		40.98	0.16	40.85	0.35
NOAA-12	AVHRR/2 (A205)	40.98	0.28	40.01	0.48
NOAA-14	AVHRR/2 (A204)	41.43	0.45	41.79	0.36

* Two cycles of laboratory measurements were performed for the AVHRR/2 flown on *NOAA-11*: (top row) one in Jul 1981 and the other (bottom row) in Nov 1987, about 1 yr before launch.

a better digitization that allows a more accurate estimation of the true mean and true STD from the digitized SC data. Mitchell (2001) and our analyses in section 5c below show that both mean and STD statistics estimated from underdigitized SC data may be biased with respect to their true values. It is therefore possible that the large differences between the σC_{Si} parameters for different instruments in Table 1, and between the two calibrations for the same instrument (see *NOAA-11* example in Table 1a, when two calibration were conducted in a 6-yr interval) are only partly due to instrument differences/aging and partly due to digitization in the SC. For the AVHRR/3 instruments, more comprehensive statistics of the SC have been collected and processed than was done before (ITT 1997, 1999, 2002). These statistics (not shown here) clearly indicate that the estimates of the σC_{Si} remain highly variable and uncertain. More work is needed to reliably characterize the radiometric noise in the AVHRR channels from undersampled digitized data, the reason being that these ITT instruments do not produce enough noise for easy statistical analysis.

In the NOAA operations, however, the ZC calibration formulation by Eq. (3) is not used. Instead, a regression form of the SRB calibration equation is adopted (Kidwell 2000; Goodrum et al. 2003):

$$A_{Ei} = S_i C_{Ei} + I_i. \quad (4)$$

Here, the S_i and I_i are channel-specific calibration slope and intercept, derived through regression analyses of A_{Ei} versus C_{Ei}. The pairs of points (A_{ei}, C_{Ei}) can be measured either in laboratory (preflight) or vicariously (postlaunch). Parameters of the calibration Eq. (3) are reproduced in Table 2a for AVHRR/1 and /2 after Kidwell (2000) and in Table 2b for AVHRR/3 after Goodrum et al. (2003).

The formulations by Eqs. (3) and (4) are equivalent if $I_i/S_i \equiv C_{oi}$ (Abel 1990). However, this latter condition is not automatically ensured and leads to significant calibration errors if violated. Separate columns of Table 2 list the "equivalent zero count" values calculated as $C_{oi} = I_i/S_i$. Data in Table 2 compare well with some "preflight offset" values found in AVHRR literature (e.g., Kaufman and Holben 1993) and less favorably with some others (e.g., Teillet and Holben 1994) that might have been based on outdated preflight NOAA calibrations, which are occasionally revised. Mitchell (1996) presented a striking example of such a revision for the AVHRR/2 on board *NOAA-14*.

Comparison of Tables 1 and 2 shows that the equivalent ZC calculated from Eq. (4) may differ significantly from the measured (mean) SC. For instance, the prelaunch value of $I_3/S_3 \sim 71$ in channel 3a of AVHRR/3 on board *NOAA-16* is far off the SC measured in laboratory, $C_{S3} = 42.2$. Apart from this extreme example, the I_i/S_i are within a few tenths to a few counts of C_{Si}. It will be further shown below that the SCs change in-flight over lifetime of AVHRR instruments and differ from their prelaunch counterparts listed in Table 1. These conceptual inconsistencies lead to confusion and large data errors in the low radiances and products derived therefrom such as aerosols over ocean (e.g.,

TABLE 1b. Preflight (laboratory) measurements of mean/STD SCs for AVHRR/3 according to ITT manuals. (Note that in laboratory, a number of STDs have been measured. The ITT reports their mean/min/max/std statistics. Only mean STD is shown below.)

Platform	Instrument	Band 1 (λ_1 = 0.63 μm)		Band 2 (λ_2 = 0.83 μm)		Band 3A (λ_3=1.61 μm)	
		C_{S1}	σC_{S1}	C_{S2}	σC_{S2}	C_{S3}	σC_{S3}
NOAA-15	AVHRR/3 (A302)	38.0	0.26	38.0	0.21	39.9	0.63
NOAA-16	AVHRR/3 (A301)	38.9	0.27	38.0	0.06	42.2	0.80
NOAA-17	AVHRR/3 (A304)	39.9	0.31	39.8	0.19	40.9	0.48

TABLE 2a. Preflight calibration slopes S_i and intercepts I_i in calibration Eq. (3) for AVHRR/1 (flown on board TIROS-N and *NOAA-6*, *-8*, and *-10*) and AVHRR/2 (flown on board NO*AA-7*, *-9*, *-11*, *-12*, and *-14*) (Kidwell 2000) and "equivalent zero counts" derived as $C_{oi}=I_i/S_i$.

	Band 1 (λ_1 = 0.63 μm)			Band 2 (λ_2 = 0.83 μm)		
	S_1	I_1	C_{o1}	S_2	I_2	C_{o2}
TIROS-N	0.1071	−3.9000	36.41	0.1051	−3.5000	33.30
NOAA-6	0.1071	−4.1136	38.41	0.1058	−3.4539	32.65
NOAA-7	0.1068	−3.4400	32.21	0.1069	−3.4880	32.63
NOAA-8	0.1060	−4.1619	39.26	0.1060	−4.1492	39.14
NOAA-9	0.1063	−3.8464	36.18	0.1075	−3.8770	36.07
NOAA-10	0.1059	−3.5279	33.31	0.1061	−3.4766	32.77
NOAA-11	0.0906	−3.7300	41.17	0.0900	−3.3900	37.67
NOAA-12	0.1042	−4.4491	42.70	0.1014	−3.9925	39.37
NOAA-14	0.1081	−3.8648	35.75	0.1090	−3.6749	33.71

Mitchell 1996, 2001; Geogdzhayev et al. 2002; Mishchenko et al. 2003; Ignatov et al. 2004), and therefore need to be resolved.

c. Sensitivity of reflectances and aerosol optical depths to ZC

At this point, it is relevant to scale the AVHRR response in terms of reflectances and products derived there from such as aerosol optical depth (AOD), τ. According to Eq. (4), one count is equivalent to S_i (%) reflectance. Kidwell (2000) shows that for the AVHRR/1 and/2 SRBs, $S_i \sim 0.1\%$, and Goodrum et al. (2003) show that for the AVHRR/3, $S_i \sim 0.05\%$ in bands 1 and 2, and 0.025% in 3A. For aerosol retrievals from AVHRR/2 at a typical Sun-view geometry, a ~0.1% reflectance error is approximately equivalent to an AOD error of $\delta\tau \sim 0.02$ (e.g., Ignatov 2002, 2003). For AVHRR/3, the sensitivity is a factor of 2 smaller in bands 1 and 2 ($\delta\tau \sim 0.01$), and a factor of 4 smaller in band 3A ($\delta\tau \sim 0.005$). These values should be compared with the typical τ signals over ocean, from $\tau \sim 0.12$ in AVHRR band 1 (equivalent to a relative error of ~16% and ~8% for the AVHRR/2 and/3, respectively) to $\tau \sim 0.08$ in AVHRR/3 band 3A (6% relative error). In the above-mentioned extreme example with *NOAA-16* AVHRR/3, when the prelaunch ZC in band 3A was off by $\Delta C_{o3} \sim +30$ count, the AOD was biased low by $\Delta\tau_3 \sim -0.14$ (see Figs. 5 and 6 in Ignatov et al. 2004). As a result, more than 90% of the global τ_3 data in this band turned negative, rendering the AOD product from this band unusable for any aerosol studies. The aerosol size parameter such as the Ångström exponent is even more sensitive to radiometric uncertainties than AODs (Ignatov 2002). Using a correct ZC is thus vital to ensure the quality of aerosol product over ocean. This paper is to show that specifying a more accurate ZC from the AVHRR SC information is quite realistic.

3. AVHRR space count measurement setup

a. AVHRR data collection

The AVHRR data collection is achieved by a synergetic use of two subsystems, optical and electronic. The optical subsystem scans cross-track by a continuous 360° rotation of the beryllium mirror in a clockwise direction at a speed of 360 rotations per minute (or 6 rotations per second). This results in an east-to-west traversal when a platform "ascends" from south to north, and in a west-to-east traversal when it "descends" from north to south. Meanwhile, the view electronics keeps sampling the radiation reflected from the mirror continuously, at a frequency of $f \sim 40$ kHz. The samples are adjacent in time, so that the "time window" of the AVHRR view electronics is $\Delta\tau_V = 1/f \sim 25 \times 10^{-6}$ s = 25 μs, corresponding to a "mirror angle window," $\Delta\theta_V \sim 0.054°$.

While in three sectors of the mirror angle (called the space view, SV; Earth view, EV; and blackbody view; BV), the output voltage from the view electronics is digitized and recorded. One recorded sample is called an "AVHRR count" or "pixel." The time constant

TABLE 2b. Preflight calibration slope S_i and intercept I_i in calibration Eq. (3) for AVHRR/3 (low gain) flown on board NOAA–KLM satellites (Goodrum et al. 2003) and the equivalent zero counts derived as $C_{oi}=I_i/S_i$. (Note that the calibration slopes on AVHRR/3 are smaller by a factor of 2–4, compared to AVHRR/1 and /2, due to implementing the dual-slope concept.)

	Band 1 (λ_1 = 0.63 μm)			Band 2 (λ_2 = 0.83 μm)			Band 3A (λ_3 = 1.61 μm)		
	S_1	I_1	C_{o1}	S_2	I_2	C_{o2}	S_3	I_3	C_{o3}
NOAA-15	0.0568	−2.1874	38.51	0.0596	−2.4096	40.43	0.0275	−1.0684	38.85
NOAA-16	0.0523	−2.0160	38.55	0.0513	−1.9430	37.88	0.0287	−2.0430	71.18
NOAA-17	0.0555	−2.2193	39.99	0.0543	−2.1227	39.09	0.0265	−1.1153	42.09

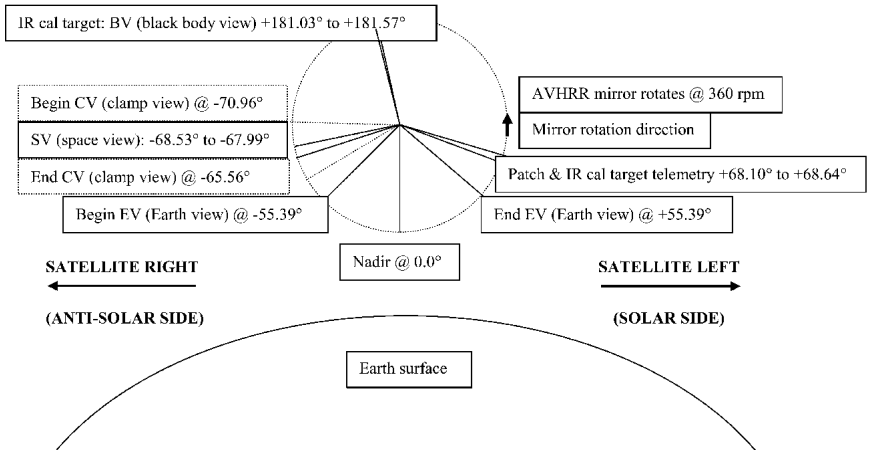

FIG. 1. Schematic of one full AVHRR scan (not to scale). [Represents a compilation from Figs. 1.2–3 of ITT (1997); Fig. 1.10 of Cracknell (1997); Fig. 1 of Cao et al. (2001); and Fig. 7.1.2.2–1 of Goodrum et al. (2003).] The direction of satellite motion is oncoming (perpendicular to the plane of the drawing). AVHRR mirror rotates clockwise, at a rate of 360 rotations per minute, or 6 rotations per second. Rotation cycle begins with line synchronization at −73.99° mirror angle (not shown). The relevant sectors/number of samples are CV (−70.96° to −65.56°)/1*; SV (−68.53° to −67.99°; found exactly in the center of the CV sector)/10 SV; EV (−55.39° to +55.39°)/2048; BV (+181.03° to 181.57°)/10. (*The clamp view sample has ~100 longer time constant compared to the space/Earth/blackbody views and is not recorded on board.)

("memory") of the AVHRR view electronics, τ_V, is very small compared to its time window ($\tau_V \ll \Delta\tau_V$). As a result, the view electronics fully "forgets" the previous pixel signal by the time it gets to the next one.

A schematic of one full AVHRR mirror revolution is presented in Fig. 1. A new cycle begins with line synchronization when the mirror points at $\theta = -73.99°$ (not shown). An idle sector follows ($N = 101$ samples not recorded), then $N = 10$ SCs are recorded while the mirror is in the angle range from $\theta = -68.53°$ to $-67.99°$. A new idle sector follows from $\theta = -67.99°$ to $-55.39°$ ($N = 233$), after which $N = 2048$ EV pixels are recorded (from $\theta = -55.39°$ to $+55.39°$). After some more idle samples and auxiliary information sectors (such as, e.g., the PRT temperatures; not shown in Fig. 1), $N = 10$ BCs are recorded while mirror scans from $\theta = +181.03°$ through $+181.57°$.

The full-resolution data format is also referred to as the local area coverage (LAC). In global area coverage (GAC) format, the same number of SCs/BCs per scan line is kept ($N = 10$), but only 409 EV pixels per line are sampled (each representing an average of 4 LAC pixels out of every 5), and only every third line is saved (resulting in two GAC lines per second). The data analyzed in this study are all GAC.

b. Space count measurements

The location of the space-view sector on the satellite right was chosen to avoid the Sun, which is always found on the satellite left. Contamination from the solar light reflected by different elements of the satellite body (the "stray light") has been minimized too. The Moon, however, appears occasionally in the AVHRR space-view sector. This is discussed in C. Cao et al. (2004, unpublished manuscript) and in section 4 below.

The AVHRR has been designed to maintain an approximately constant level of SC ~ 40 in the SRBs, and ~990 in the EEBs.[4] The choice of the specific numbers is historical, for instance, a different value of SC ~ 29 is used in the SRBs of the imagers and sounders flown on board the geostationary satellites. Setting a "pad" at the bottom/top of the radiometric scale (the "leg/head room") helps avoid the out-of-scale readings that may occur due to aging/degradation of the AVHRR optoelectronic subsystem, and to enable noise measurements.

c. Clamping

Clamping is a feedback mechanism by which the whole AVHRR radiometric scale is continuously self-adjusted by a slow (*additive*) shifting in such a way that the ZC pedestal in the SRBs is maintained at an approximately constant level of 40 counts.

First, a "clamp count" (CC) is measured (but *not* recorded on board). It differs from the SC due to 1) sampling over a wider time/angle window, and 2) pro-

[4] Note that there are *two different* clamping electronics on the AVHRR: one circuit is used with the SRBs, and the other with the EEBs. In a context of the present study, the SRB clamping is of interest and analyzed below.

cessing through different clamp electronics. The desire to have a less noisy CC led to setting the clamp window much wider, with $\Delta\tau_C \sim 100\Delta\tau_V \sim 2500$ μs, though centered exactly at the center of the space window (see Fig. 1). The clamp electronics samples only once per mirror rotation cycle.

Next, the CC is compared to a preset value of 40, and a feedback signal proportional to the difference is generated and propagated back to negate the deviation. The feedback propagates slowly, so that the SC measured in the beginning of the cycle continues to hold over at least one full mirror revolution ($T \sim 1/6$ s). The time constant of the clamp feedback circuit is $\tau_C \sim 11$ s $\gg T \sim 1/6$ s (see section 4c for the detail on how the τ_C was estimated).

d. Implications of clamping on the SC data

In a stationary mode (i.e., absence of any perturbations to the SV/CV, such as caused by the Moon), the average SC may differ from 40 systematically. This is because the average brightness in the (wider) CV window may differ from the brightness in the (narrower) SV window, or the two electronics may process the same input differently or both. Long-term trends in the SC may develop 1) if the differences between the clamp/space windows change systematically in time (due to, e.g., systematic orbit evolution; see Ignatov et al. 2004), 2) because clamp/space electronics age differently, or 3) both. Short-term perturbations in the SC may result from a bright object (Moon) quickly traversing the space and/or clamp view as discussed in section 4 below.

The relevant question is whether those observed SC features are "real" or not—that is, should the on-orbit measured SC be used to specify the ZC in Eq. (3) or should a constant (e.g., prelaunch) value be used instead? We argue that the onboard measured SC should be used during periods when the SC does not experience sharp variations (see examples in section 4). The situations when the SC quickly changes from line to line should be flagged out and excluded from the Earth-view data analyses.

4. Examples of the Moon effect on space count

The (narrower) space and the (wider) clamp views are both supposed to observe deep space, free of bright objects. Periodically, however, one of them or both point to the Moon or part of it, which may additionally be in different phases. Effect of lunar contamination on the calibration of the advanced microwave sounding unit (AMSU; also on board NOAA platforms) has been documented by Kigawa and Mo (2002), and similar AVHRR analyses are currently under way (C. Cao et al. 2004, unpublished manuscript). Here, a few Moon examples are considered to help understand the AVHRR space view and clamping mechanism. The fact

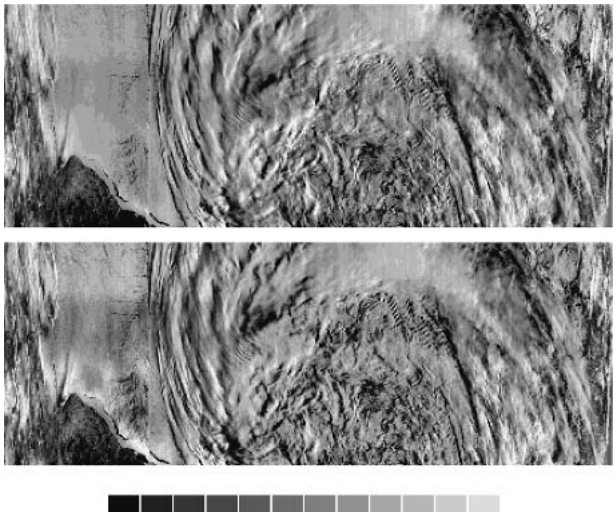

FIG. 2. Detrended/normalized Earth-view count (see section 4a for definitions) in AVHRR bands (top) 1 and (bottom) 2, for a ~75 s (150 lines) fragment of a *NOAA-15* GAC orbit on 19 Apr 2000 (1325 UTC). Image (150 lines × 409 pixels) is of the east coast of Hudson Bay in Canada, centered at 60°N, 78°W. *NOAA-15* descends (top) north to (bottom) south and scans (left) west to (right) east. The palette corresponds to −3 to +3 detrended/normalized count in steps of 0.5. Depressed Earth-view count in both bands over $\Delta l \sim 50$ lines is due to Moon contamination. Line numbering is arbitrary.

that the Moon-induced variations in the SC are clearly echoed in the Earth-view data illustrates the major point of this study, namely, that the in-flight measurements of SC must be used to specify the calibration offset in the Earth-view data.

a. Moon anomaly in the SC: Effect on the Earth-view data

Figure 2 maps the Earth-view counts[5] in AVHRR/3 bands 1 and 2, for a ~75 s fragment of a *NOAA-15* GAC orbit on 19 April 2000 (1325 UTC). The image of $L \times K$ [$L = 150$ lines; $K = 409$ pixels] centered at 60°N, 78°W, was taken over the east coast of the Hudson Bay in Canada, while *NOAA-15* was descending from north to south, scanning from west (left) to east (right). The local time increases across the image from ~0715 LST on the left to ~0915 LST on the right, and so does the illumination of the scene. To mitigate the large meridional trends in the scene illumination, the image was first detrended (by calculating mean count over $L = 150$ lines for each pixel, $k = 1$ to 409, and subtracting it from each count in the respective column) and then

[5] Recall that for the AVHRR/3 SRBs, the low gain is in effect for counts from 0 to 510 (note that all SCs fall in this gain), and the high gain is in effect from 510 to 1024 (see footnote 3). As a result, the radiance weight of counts <510 and >510 differs by roughly a factor of 2. Data from both gains are present in Fig. 2. Nevertheless, the analyses in this section are done in counts, for simplicity.

normalized (by ratioing the difference to the respective column-specific STD count). Wide stripes ($\Delta l \sim 50$ lines) of depressed counts are clearly observed in both bands.

Figure 3 (top) plots a transect of the (original) EV counts in the two bands (averaged over the 409 GAC pixels within a scan line) as a function of scan line. The scene clearly shows a dip from line $l \sim 20$–70 superimposed on the general north-to-south darkening trend. Figure 3 (bottom) plots a corresponding transect of the respective SCs (averaged over 10 space views, within a scan line). The SCs are remarkably stable ($C_{S1} \sim 38.1$, $C_{S2} \sim 39.0$) before $l \sim 20$, then they dip to $C_{Si} \sim 10$, coherently in the two bands, and recover only after $l \sim 70$. The one-to-one correspondence between the SC and the EV data clearly suggests that the onboard measured SC should be used to normalize the EV count.

The episodes with rapid changes in the SC similar to those shown in Figs. 3–4 are rare and extreme, and it is safer to flag them out and exclude the corresponding EV data from analyses rather than attempt correcting them. At the same time, such "data anomalies" lend themselves to in-depth understanding of the physics of the phenomena much better than "business as usual" situations (considered in section 5).

b. *Two mechanisms of the Moon effect on space count*

Figure 4 illustrates two mechanisms of the Moon effect on the SC data. The *NOAA-15* example in Fig. 4a (replotted from bottom of Fig. 3, with averaging over 10 SCs per line removed) suggests that all individual SCs react to the Moon forcing identically. The SC first drops from ~40 to ~10 in 5–7 s, stays low for ~25 s, and then returns to its pre-Moon level after an approximately 1-min "ringing." The *NOAA-17* example in Fig. 4b features a different pattern. Here, the individual SCs react to the Moon forcing quite differently. The SC1 shows a hint of *NOAA-15*-like decline, but all other SCs increase, some of them by as much as 80 counts over the background ~40 count level. After a ~25-s interval, the SC returns to its pre-Moon level after a few oscillations, similarly to *NOAA-15*.

Figure 5 illustrates the physics behind the two different patterns of the Moon effect on the SC. Two "swaths" in the deep space shown with solid and broken lines, correspond to the AVHRR space and clamp views, respectively. Recall that the AVHRR angular "clamp-view swath" is 5.4°, 10 times wider than the "space-view swath," which is only 0.54° and comparable to the angular size of the Moon. The AVHRR records

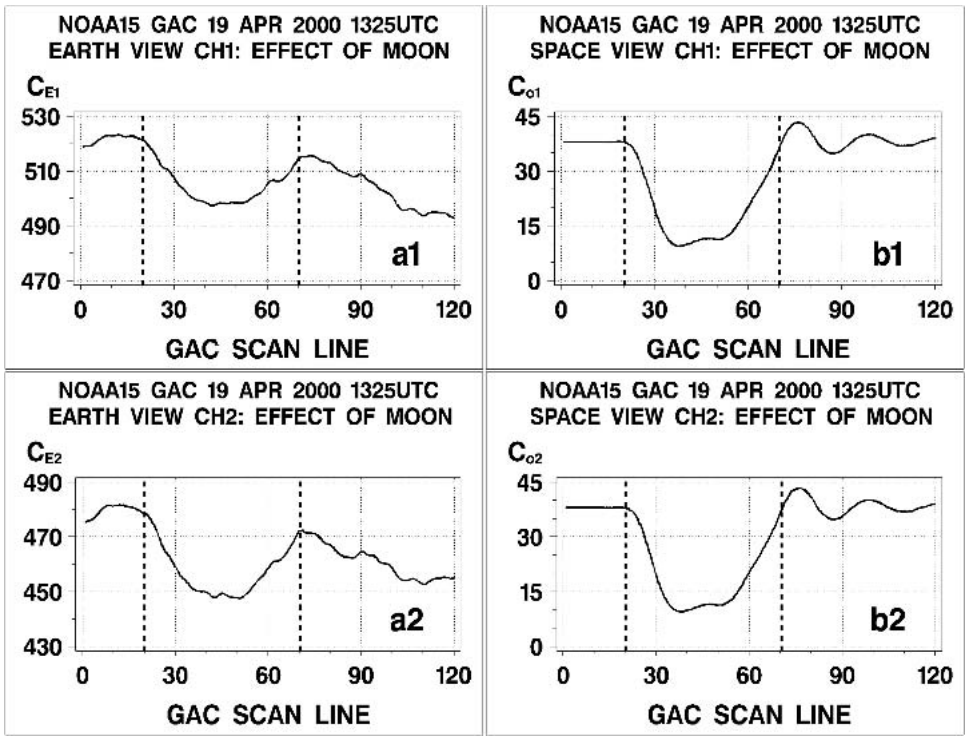

FIG. 3. (left) 1-min (120 GAC lines, starting from line 10 in Fig. 2) subset of original Earth-view count data from Fig. 2 (before detrending/normalization) in AVHRR bands 1 and 2. Each curve is average count over $N = 409$ pixels per scan line shown as a function of scan line. (right) Respective space view counts averaged over $N = 10$ pixels per scan line. Data in lines from $l \sim 20$–70 are affected by the Moon.

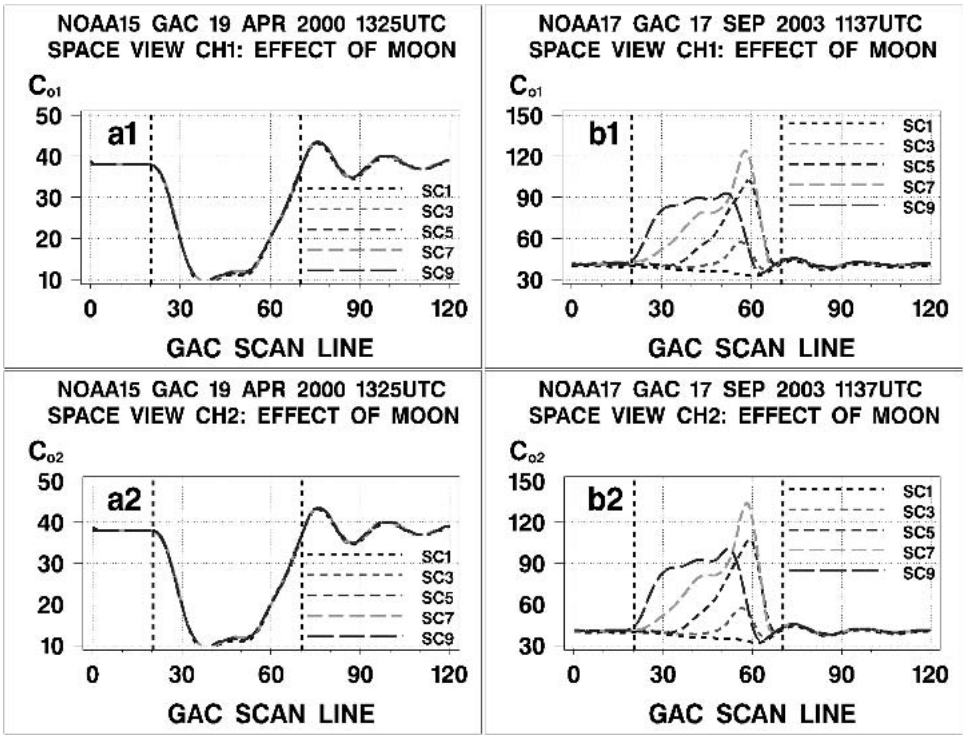

FIG. 4. Space-view counts (shown are 5 out total 10) in bands 1 and 2 of AVHRR flown on board (a) *NOAA-15* and (b) *NOAA-17*. Data in lines from $l \sim 20$–70 on both platforms are affected by the Moon.

10 SC pixels while traversing the space-view sector (one SC coming from a ~0.054° sector), but measures only one CC pixel while traversing the clamp view sector, which is not recorded.

Figure 5a shows an example when the clamp view sees the Moon but the space view does not. In this case, the clamp view works to set its brighter-than-deep-space target to 40 counts, while all 10 space views still point to the dark deep space. As a result, all 10 SCs are identical and consistently lower than 40 (cf. Figure 4a).

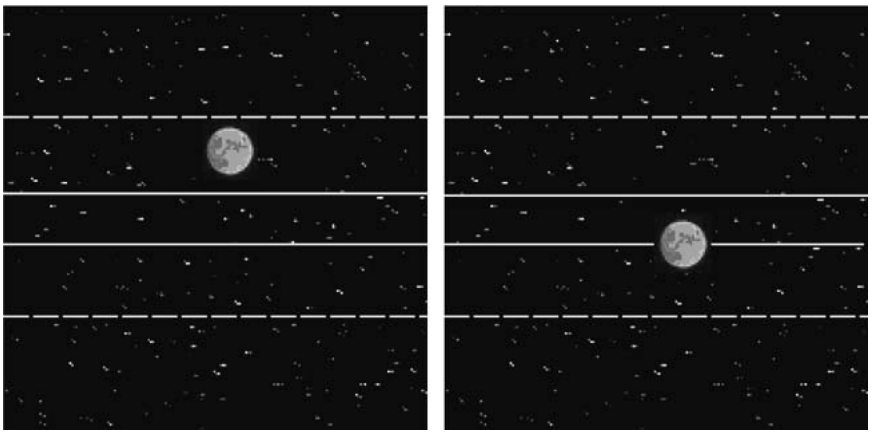

FIG. 5. Two mechanisms of the Moon effect on SC. NOAA satellite moves in horizontal left to right; AVHRR scans in vertical top to bottom. Superimposed are two swaths: by clamp view (bracketed by two broken lines; angular size ~5.4° = one clamp count) and space view (bracketed by two solid lines; angular size ~0.54° = 10 space counts, ~0.054° each). (left) Moon (~0.5° in diameter) is in the clamp swath but not in the space swath (cf. *NOAA-15* example in Fig. 4, left); (right) Moon is in both clamp and space swaths (cf. *NOAA-17* example in Fig. 4, right).

Figure 5b shows an example when both the clamp and space views see the Moon. In this case, the inertial clamp starts working to set the CC of the brighter background to 40 count, but does not finish its job before different SCs point to different parts of the bright Moon, and quickly react to it (cf. Figure 4b). It is clear that the scenario shown in Figs. 4a and 5a is much more probable, in proportion to the clamp-to-space-view sector ratio (~10).

c. Clamp circuit as underdamped oscillator

The SC data of both *NOAA-15* and *-17* in Fig. 4 show two features for line numbers $l > 70$: 1) close agreement between all 10 SCs and 2) after-ringing. This corresponds to a period when the clamp circuit undergoes free relaxation and readjusts to the normal background space brightness, after the clamp-view sector ceases seeing the Moon. Quantitative analyses of the relaxation process lends itself to estimating parameters of the clamp circuit, which is instrumental to work out an optimal strategy of utilizing the SC data to calibrate the AVHRR.

Figure 6 replots those parts of Fig. 4 with $l > 70$ with two modifications: 1) all 10 SCs are now averaged to suppress residual noise and 2) the abscissa is transformed from line number l to time t [calculated as $t = (l - 70)/2$ for the GAC data]. Superimposed is fit to the data in the form

$$x = x_o + \alpha \exp(-\gamma t) \sin(\omega t + \varphi). \quad (5)$$

Equation (5) represents the solution of the so-called oscillator equation

$$\frac{d^2x}{dt^2} + 2\gamma \frac{dx}{dt} + \omega_o^2 x = 0, \quad (6)$$

in the case of an underdamped oscillator (i.e., when $\omega^2 = \omega_o^2 - \gamma^2 > 0$). Equation (5) is generic to a number of physical processes that result in *free oscillation* (first and third terms on the left-hand side) with *damping* (second term). Examples of mechanical and thermodynamic processes include, for example, mass-spring-friction or pendulum-gravitation-friction, and gas-piston-friction oscillations. The AVHRR clamp electronics circuit can be generally viewed as an (electromagnetic) LCR oscillator with inductance L, capacitance C, and resistance R, in which case $\gamma = R/2L$, $\omega_o^2 = 1/(LC)$. In the classical LCR formulation, x represents the charge of the capacitor. In all analyses below, however, the x is considered to be the SC.

The γ parameter in Eq. (5) provides a quantitative measure of how quickly the clamp circuit forgets the

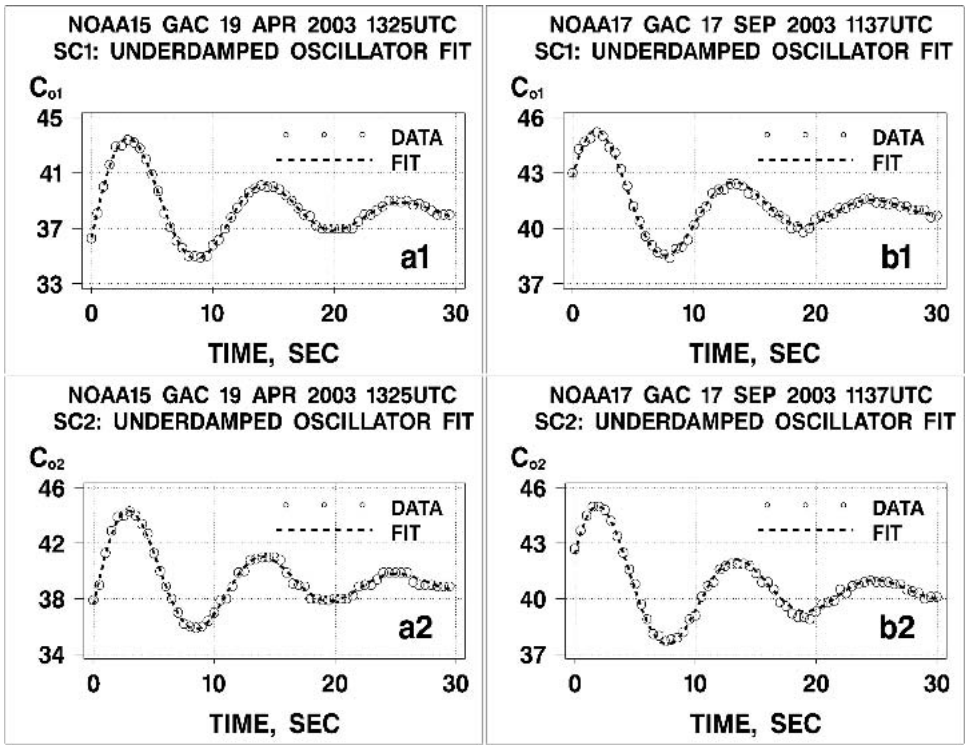

FIG. 6. Examples of relaxation of the SC (averaged over 10 SCs per line) in AVHRR bands 1 and 2 after the Moon ceases to affect the space/clamp view: (a) *NOAA-15* and (b) *NOAA-17*. Fit with Eq. (4) superimposed on the data (parameters of the fit equation listed in Table 1). Zero time corresponds to $l = 70$ in Fig. 4.

Moon disturbance and returns to the background level. The inverse-γ parameter, $\tau = 1/\gamma$, is called the *decay* or *envelope* time. The ω parameter defines the frequency of oscillations (that can alternately be expressed through the oscillation period, $T = 2\pi/\omega$). The amplitude of the perturbation, δC_{oi}, and the initial phase, φ, are specified at zero time, $t = 0$, which is defined by convention. For convenience of further analyses, Eq. (5) is rewritten as

$$C^*_{oi} = C_{oi} + \delta C_{oi} \exp\left(-\frac{t}{\tau}\right) \sin\left(\frac{2\pi t}{T} + \varphi\right). \quad (7)$$

Table 3 summarizes the fit parameters for the two examples in Fig. 6. For comparison, two adjacent *NOAA-15* orbits (denoted "−1" and "+1," respectively; not shown in Fig. 6) have also been fit with Eq. (7) and their parameters listed in Table 3. The unperturbed SCs, C_{oi}, differ from 40 in all cases by up to 2 counts. The decay time and the oscillation period ($\tau \sim T \sim 11$ s; agreement between the two is apparently by coincidence) are well reproducible between different platforms, bands, and orbits. This is expected because these parameters belong to the AVHRR clamp electronics and not to band or orbit. The amplitude of the perturbation, δC_{oi}, and the phase, φ, depend upon the initial time at which they are defined. For instance, if the initial time were specified one decay period earlier (i.e., at $t \sim -\tau$), then the value of δC_{oi} would be ~2.7 times larger. This explains the difference between the δC_{oi} in Table 1, and its visual estimate from Fig. 4 (~30 counts in *NOAA-15* and ~80 counts in *NOAA-17* data).

In practical perspective, the δC_{oi} and τ estimates in Table 3 suggest that it takes from 50 to 75 s to reduce the perturbation in the SC by two to three orders of magnitude. Combined with a ~25 s length of the Moon event itself, this suggests that from 1–2 min of data should be discarded. Comparison of the three consecutive orbits of *NOAA-15* suggests that Moon contamination persists over a few orbits. A detailed procedure to identify and exclude moon-contaminated data is currently being developed and will be reported elsewhere.

5. Typical SC suborbital variability: Case studies from *NOAA-15* and *-16*

Several individual orbit analyses in this section show how the SC behaves under "business as usual" conditions. The SC statistics in AVHRR bands 1 and 2 are further compared with larger statistics of the night count (NC). The two statistics compare well, suggesting that these two bands are not affected by thermal leaks (Ignatov 2003) and that the NCs may be used in lieu of the SCs.

a. Two NOAA-15 examples

Figure 7 plots the histograms of SC in the two AVHRR/3 SRBs for two GAC orbits on 21 June 1999 and 23 October 2001 (N = 108 840 and 124 400 SCs, corresponding to N = 10 884 and N = 12 440 scan lines, respectively) of a morning satellite *NOAA-15* (nominal equator crossing time 0730/1930 LST). No data are available in band 3A, which was discontinued shortly after launch of *NOAA-15*. The SC is within a three-count range in band 1 (from 37 to 39), and within two-count range in band 2 (from 38 to 39). However, their relative proportions differ for the two orbits separated by 28 months, resulting in different sampling mean and STD statistics. Mitchell (2001) and analyses in section 5c below show that sampling statistics estimated from the digitized SC may be biased with respect to the true ZC.

The EV data in the SRBs collected on the dark side of orbit may be used as a surrogate for the SC, when not affected by the Sun—for example, when sun zenith angle is $100° < \theta_o < 170°$. The night counts (NCs) are expected to be close to the SCs [if not affected by the thermal radiation leaking from a secondary peak in band's spectral response function as it is the case with some bands of the, for example, Visible and Infrared Scanner (VIRS) flown on board the Tropical Rainfall Measuring Mission (TRMM) satellite, or the Moderate Resolution Imaging Spectroradiometer (MODIS) flown onboard *Terra* and *Aqua* satellites, e.g., Ignatov 2003]. The NC histograms and statistics are superimposed in Fig. 7. There are N = 2 028 852 and N = 1 713 603 NCs in the respective orbits, a factor of ~14 to ~19 increase

TABLE 3. Fit parameters of Eq. (7). The orbits denoted with 0 have been analyzed in Figs. 4 and 6. Two adjacent *NOAA-15* orbits (preceding orbit 0, and following it) have been also processed, to estimate the interorbital evolution of the Moon effect.

	Band	Orbit	C_{oi}	δC_{oi}	τ (s)	T (s)	φ (rad)	σC_{oi}
	1	−1	38.1 ± 0.1	8.0 ± 0.7	11.1 ± 1.3	11.4 ± 0.2	−0.58 ± 0.06	0.13
	1	0	38.1 ± 0.1	7.0 ± 0.7	11.7 ± 1.7	11.3 ± 0.2	−0.26 ± 0.07	0.13
	1	+1	38.1 ± 0.1	6.1 ± 0.6	11.3 ± 1.5	11.3 ± 0.3	+0.73 ± 0.11	0.13
	2	−1	39.0 ± 0.1	8.2 ± 0.7	10.5 ± 1.2	11.1 ± 0.2	−0.56 ± 0.06	0.18
Sample 1	2	0	39.0 ± 0.1	6.9 ± 0.7	11.3 ± 1.7	11.1 ± 0.2	−0.22 ± 0.08	0.21
NOAA-15	2	+1	39.0 ± 0.1	6.1 ± 0.5	10.6 ± 1.5	11.1 ± 0.3	+0.76 ± 0.11	0.18
Sample 2	1	0	41.0 ± 0.1	5.2 ± 0.6	10.7 ± 1.9	11.4 ± 0.3	0.34 ± 0.12	0.15
NOAA-17	2	0	40.4 ± 0.1	5.5 ± 0.6	11.7 ± 1.8	11.5 ± 0.3	0.38 ± 0.11	0.15

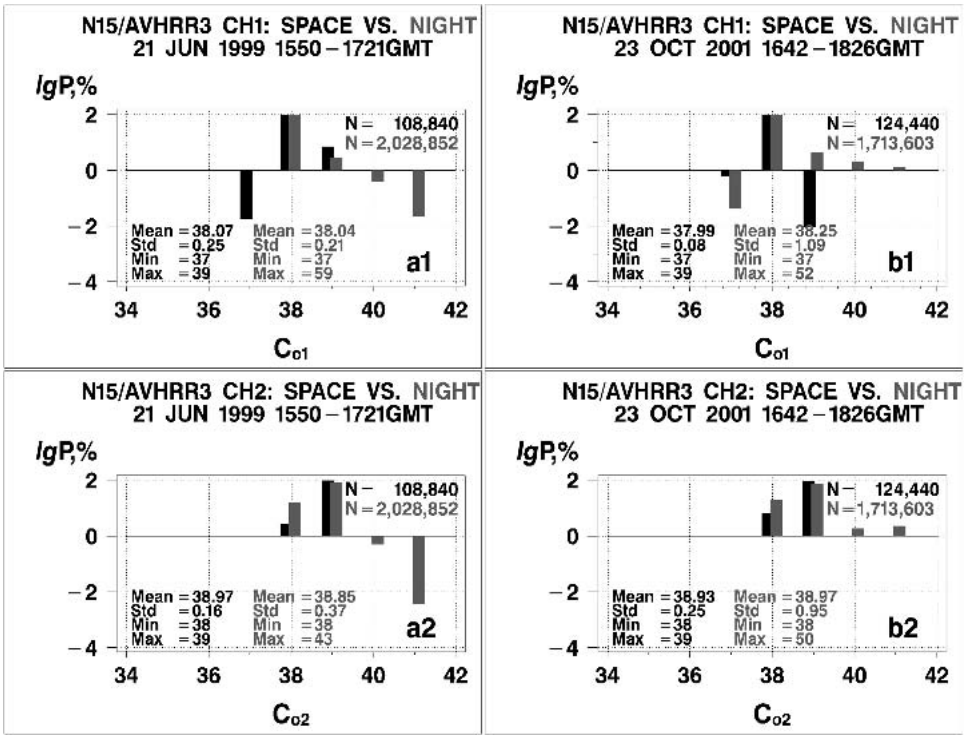

FIG. 7. Histograms of space count (black) and night count (gray) in bands 1 and 2 of AVHRR/3 flown on board *NOAA-15*, for two orbits of data: (a) 21 Jun 1999 and (b) 23 Oct 2003. The *y* axis is in logarithmic scale. General statistics of the SC and NC (number of data points, mean, and STD) are superimposed. Data in AVHRR/3 band 3A (1.61 μm) are not available as this band was discontinued shortly after launch of *NOAA-15*.

over the SC statistics. Note that there are 409 EV counts per scan line compared to the 10 SCs, a factor of ~41 increase in sample size, of which some EV data are collected during day. The NC shows more outliers compared to the SC, which are relatively easy to screen out. Note however that even before any quality control, the mean NC compares to the mean SC to within an ~0.1 count. Comparing the SC/NC statistics from the two orbits does not reveal any statistically significant change over a period of 28 months.

b. Two NOAA-16 examples

Figure 8 plots the histograms of SC in the two AVHRR/3 SRBs for two GAC orbits on 1 October 2001 and 29 September 2003 (N = 134 010 and 125 330 SCs, corresponding to N = 13 401 and N = 12 533 scan lines, respectively) of an afternoon satellite *NOAA-16* (nominal equator crossing time 1400/0200 LST). Data in band 3A are available for the first orbit but not for the second one as this band was discontinued on 1 May 2003. The SCs exhibit more variability in all SRBs compared to *NOAA-15*, but continue to compare well with the NCs. In bands 1 and 2, the high SC data are deemed to be outliers and should be screened out. In band 3A, however, the spread is apparently due to the real radiometric noise that appears to be a factor of 1.5 higher compared to its preflight estimate of 0.8 count in Table 1b. This noise far exceeds the effect of digitization (see section 5c below), making the estimates of mean and STD SC in this band quite reliable. Note that no night data are available in this band as 3A automatically switches over to 3B at the terminator (θ_o = 90°). Comparing the two orbital statistics reveals that both SC and NC degraded by a 0.2–0.3 count over the 2-yr time period.

c. Effect of digitization in SC on the estimate of ZC

The above analyses show that short-term variability in the SC is typically restricted to within two to three counts, even in the AVHRR/3 data that are digitized a factor of 2–4 finer compared to the AVHRR/1 and /2, suggesting that the improved AVHRR/3 digitization is still insufficient to resolve its radiometric noise. This hampers accurate estimate of the ZC parameter in Eq. (3), especially the radiometric noise, from the sample mean and STD of the digitized SC.

The magnitude of the resulting errors was estimated using a simple model, in which the ZC is given by a Gaussian distribution, with a "true" mean ZC, C_o, and "true" radiometric noise, σ_{Co} (cf. Mitchell 2001). A

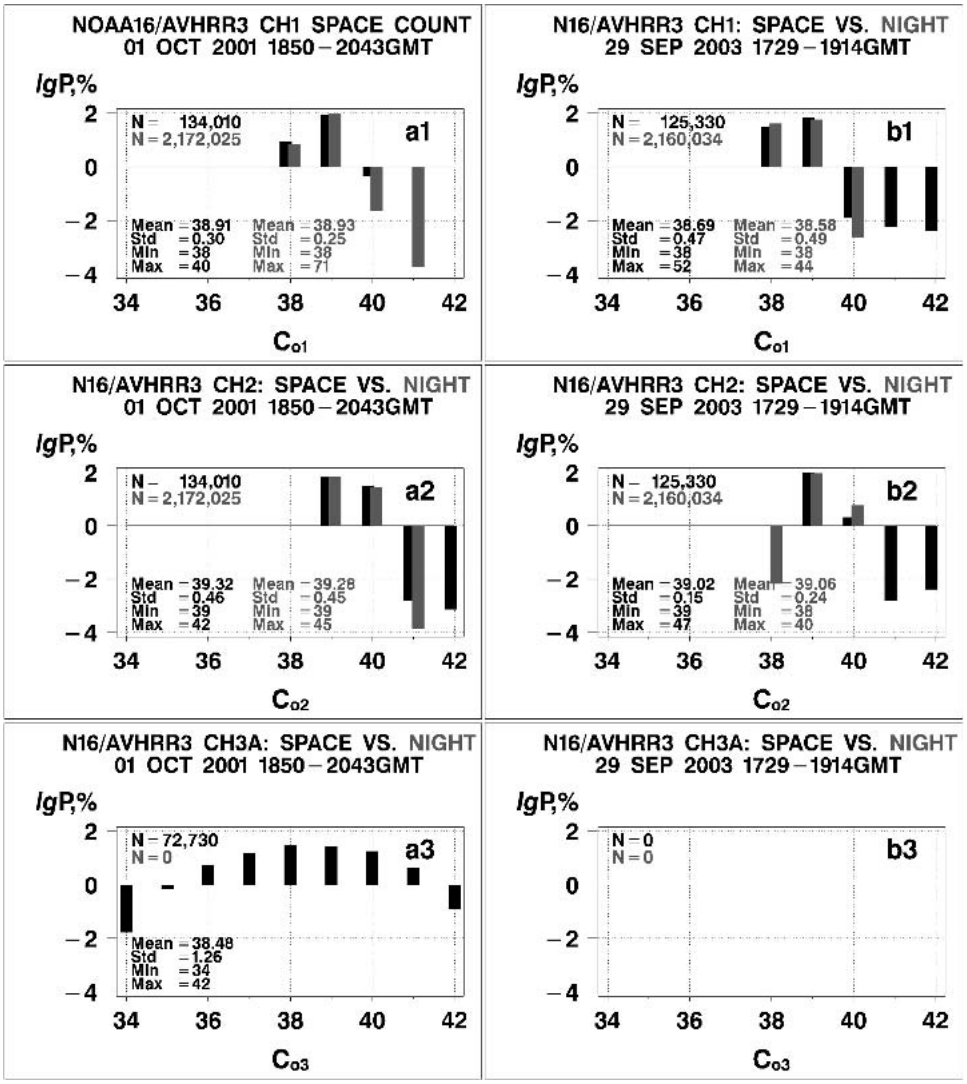

FIG. 8. Same as in Fig. 7 but for two *NOAA-16* datasets: (a) 1 Oct 2001 and (b) 29 Sep 2003. The SC data in AVHRR/3 band 3A (1.61 μm) are available in the first dataset but not in the second one, as this band was discontinued on 1 May 2003. The night count data are not available in band 3A as it switches to 3B automatically when sun angle goes over $\theta_o = 90°$.

number of model datasets, with $N = 100\,000$ ZCs each, have been generated for a number of the parameters, C_o from 39.0 to 41.0 in step of 0.1, and σ_{Co} from 0 to 0.3 in step of 0.1 that are representative of the typical AVHRR values (cf. Table 1b). The resulting real value ZCs have been then rounded to the nearest integer to simulate the discrete set of the SCs. Then the sample mean and sample STD have been calculated over the sets of integer SCs, and errors, δC_o and $\delta\sigma_{Co}$, calculated as deviations from the respective true input values, C_o and σ_{Co}.

Figure 9 plots the errors in the mean and STD ZC, $\delta C_o(C_o)$ and $\delta\sigma_{Co}(C_o)$, as functions of the true ZC, C_o. The four curves in each figure correspond to the four true STD ZC, σ_{Co}. As expected, both functions, $\delta C_o(C_o)$ and $\delta\sigma_{Co}(C_o)$, are periodic, with a period of 1 count.

If the radiometric noise is small, that is, $\sigma_{Co}\rightarrow 0$, the error in the mean ZC is largest (solid line in Fig. 9a). The error reaches $\pm$½ count for the near-half integer true ZCs (e.g., ~39.5), when those get rounded to the nearest integer SC (either 39 or 40). Typically, there is no error in the STD ZC associated with the low-noise regime, when $\delta\sigma_{Co}\rightarrow 0$ (solid line in Fig. 9b), except for the near-half integer ZC case (e.g., ZC ~ 39.5), when even a small nonzero noise may lead to the SC flipping between 39 and 40, resulting in nonzero σ_{CS}, with a maximum error in estimated STD ZC of $\delta\sigma_{Co} = 0.5$. With increased radiometric noise, maximum errors in the mean and STD ZC decrease from this worst-case

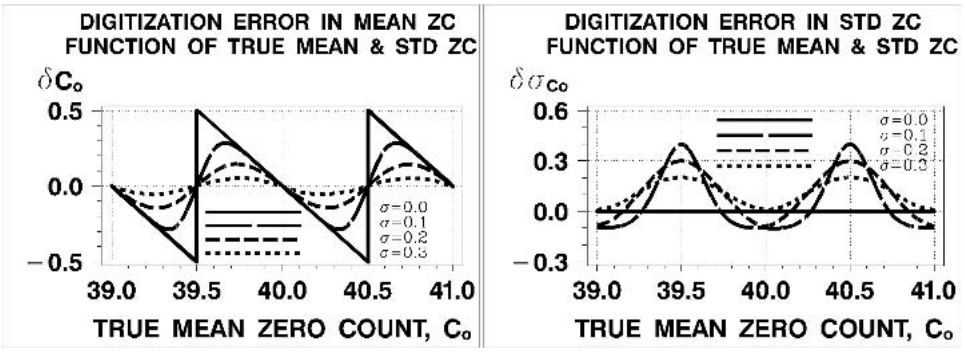

FIG. 9. Model estimate of the digitization error in the mean and STD SC statistics as a function of "true" ZC for a few levels of the true radiometric noise. For details, see section 5c.

scenario: $\delta C_o \sim 0.28$, $\delta\sigma_{Co} \sim 0.4$ for $\sigma_{Co} = 0.1$; $\delta C_o \sim 0.14$, $\delta\sigma_{Co} \sim 0.3$ for $\sigma_{Co} = 0.2$; and $\delta C_o \sim 0.05$, $\delta\sigma_{Co} \sim 0.2$ for $\sigma_{Co} = 0.3$.

These errors in the estimated ZC statistics are significant; in particular, the error in the STD ZC may exceed the true STD ZC itself. This suggests that the respective prelaunch (in Table 1) and on-orbit (in section 6) SC statistics may deviate from the actual ZC, and in particular, may not be representative of the true radiometric noise of the AVHRR instrument. Unfortunately, there is no way to narrow down this uncertainty in the estimated ZC parameters, provided the noise-to-digitization ratio remains unchanged. A different mathematical procedure was proposed by Mitchell (2001), based on fitting a Gaussian curve to the SC histogram consisting of only 2 to 3 counts. More analyses are needed to prove that this mathematical maneuver helps resolve the problem, which by its nature is ill-posed. The only way to reduce the digitization-induced error is to measure the SC at a finer digitization (say 12 bits instead of the current 10 bits). An indirect way to effectively increase digitization is to decrease the AVHRR calibration slope, S_i [see Eq. (4)] for those periods when the SC measurements are taken, because the σ_{Co} parameter increases in inverse proportion to the S_i. For instance, numerical estimates show that for $\sigma_{Co} = 3$ counts, $\delta C_o \sim 0.001$ and $\delta\sigma_{Co} \sim 0.02$. It is expected, intuitively, that the digitization error in the ZC statistics becomes negligible when the digitization effect becomes small compared to the radiometric noise.

6. Space count statistics from 1994 to present

In 1994, NOAA has implemented a system to monitor the orbital and daily SC statistics in-flight. The mean and STD SC are reported online at http://www.osdpd.noaa.gov/PSB/PPP/CALIB/home.html and archived for future use. Section 6 documents these post-1994 data. (Pre-1994 SC data are yet to be processed into compressed statistics.)

a. NOAA-9, -11, -12, and -14 AVHRR/2

NOAA-9 SC data are available for a 1-yr period from February 1994 to February 1995 (Fig. 10). In-flight values of the SCs differ by a 1.0–2.9 count from their preflight measurements and from the effective ZCs (listed in Tables 1 and 2). The SC in band 1 is more variable over time and noisier than the preflight estimates suggest. In band 2, noise is substantially lower compared to the preflight values.

NOAA-11 SC data are available from December 1993 to September 1994 (Fig. 11). The SCs differ from the preflight estimates of SC and effective ZC by a 1.1–1.8 count, and show a change of 0.4 counts in less than a year in band 2. Both bands are noisier compared to prelaunch estimates.

NOAA-12 SC data are available from December 1993 to December 1999 (Fig. 12). The SC was very stable in band 2, but noisy and variable in band 1, where it climbed 0.4 counts over the 5-yr period. Band 2 is noisier compared to the prelaunch estimates.

NOAA-14 SC data are available for over 8 yr from December 1993 to the present (Fig. 13). Both channels of AVHRR/2 show excellent stability, with $C_{S1} \sim 41$ and $C_{S2} \sim 41$, and compare well with the preflight SCs (within 0.4–0.8 count) but not with the equivalent ZCs (a 5.2–7.8 count difference; cf. Mitchell 1996). The very low noise in the *NOAA-14* SCs (below 0.05 count) suggests that this may be due to the effect of digitization, and that the true mean ZC can be probably found anywhere between ~40.8 and 41.2.

Our results for *NOAA-9*, *-11*, *-12*, and *-14* are in agreement with those by Mitchell (2001).

b. NOAA–KLM AVHRR/3

NOAA-15 was the first satellite in the KLM series to carry the AVHRR/3. The SC data are available since launch in May 1998 (Fig. 14). Its SCs are noisy yet stable over time, with average values of $C_{S1} \sim 38.0$ and $C_{S2} \sim 39.0$, and compare with prelaunch estimates of SC and effective ZC within 0–1.4 counts. The noise in

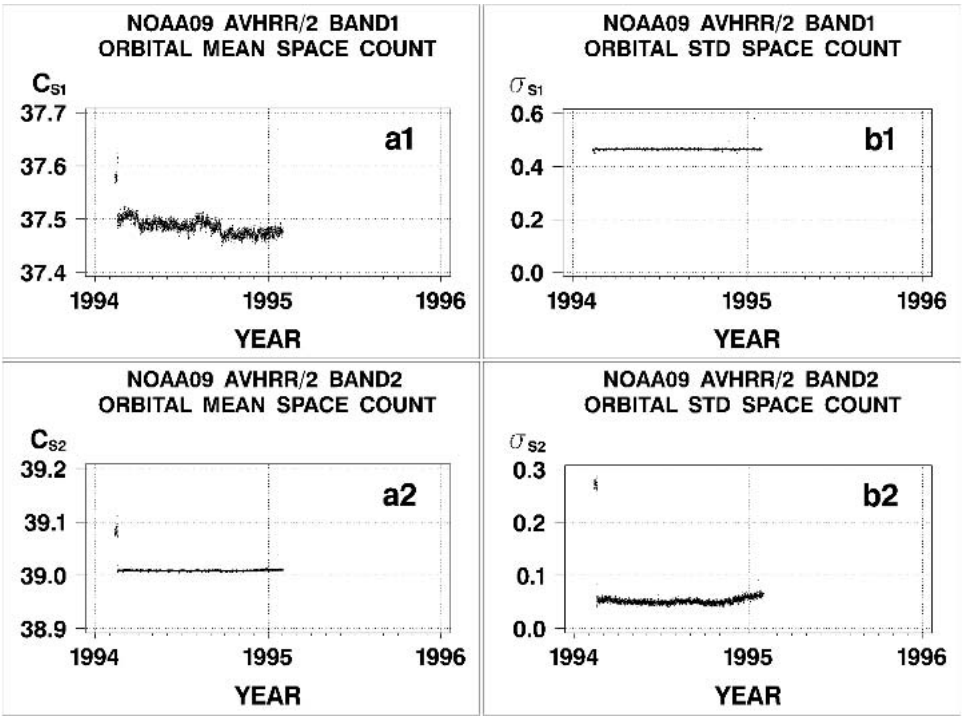

FIG. 10. Orbital (a) mean and (b) STD of space count in bands 1 and 2 of AVHRR/2 flown on board *NOAA-9* (cf. preflight SC statistics, mean, C_S, and STD, σ_S, listed in Table 1, and the effective ZC listed in Table 2). The system to monitor the SC data was implemented at NOAA in early 1994. The nature of a few outliers at the beginning of system operation is unclear. No quality control is applied to the SC data used in calculating the two statistics.

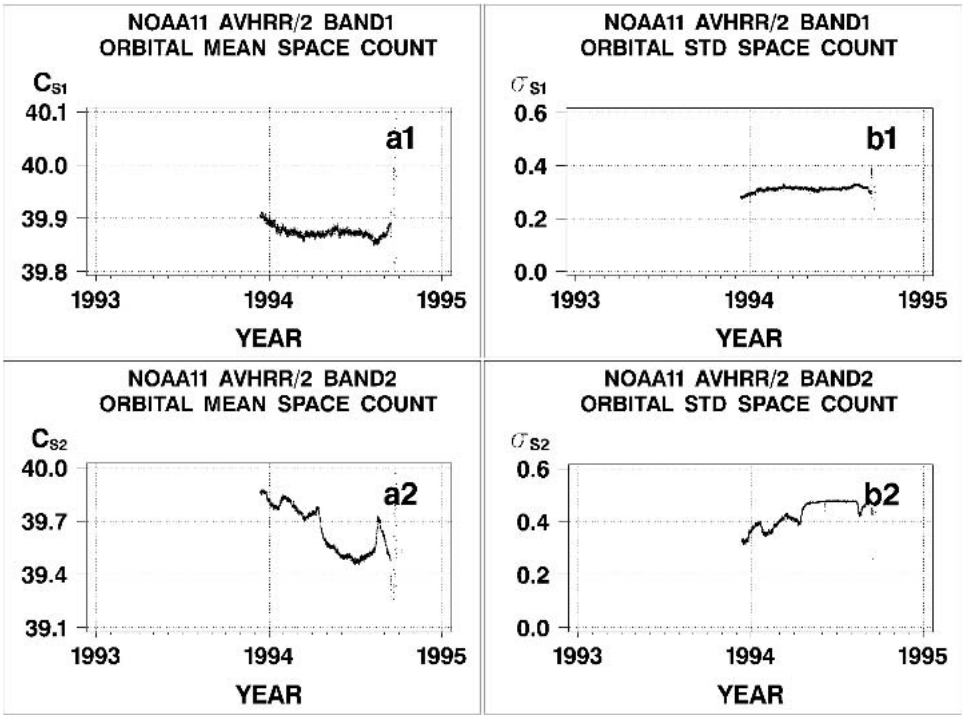

FIG. 11. Same as in Fig. 10, but for AVHRR/2 on board *NOAA-11*.

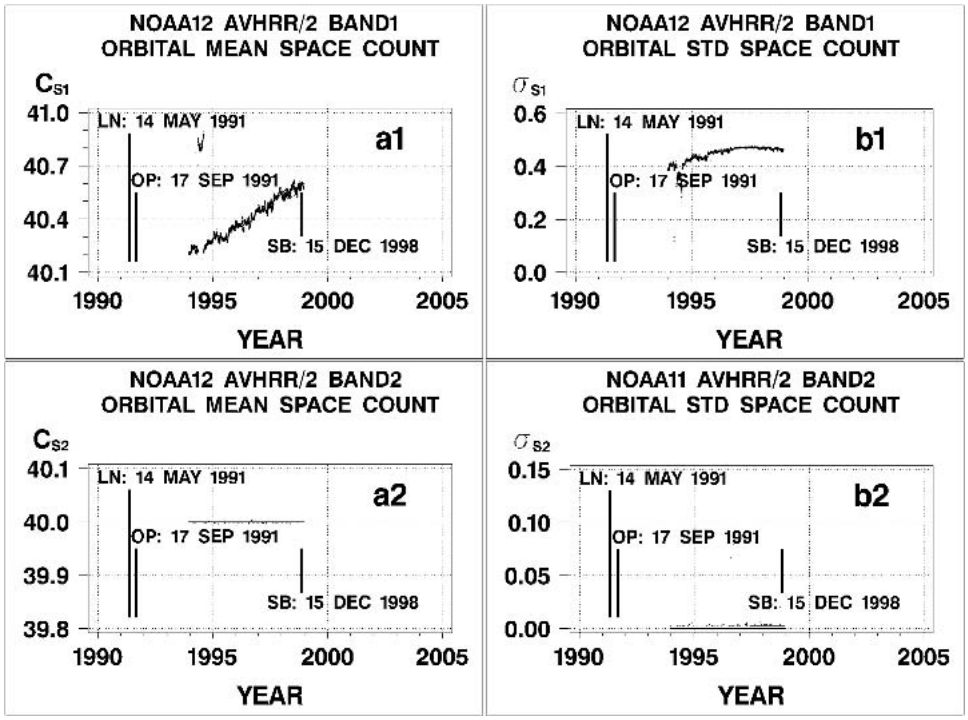

FIG. 12. Same as in Fig. 10, but for AVHRR/2 on board *NOAA-12*. Launch time (LN) and dates when the platform became operational (OP) and was put in a standby (SB) mode (i.e., served as a backup to the then operational platform) are superimposed.

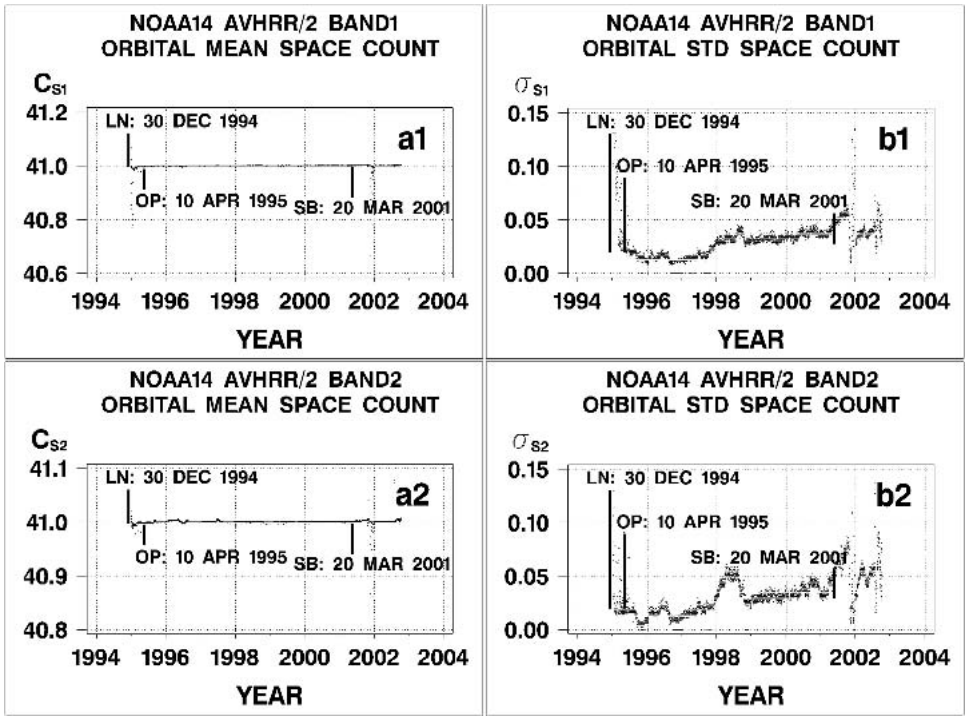

FIG. 13. Same as in Fig. 12, but for AVHRR/2 on board *NOAA-14*.

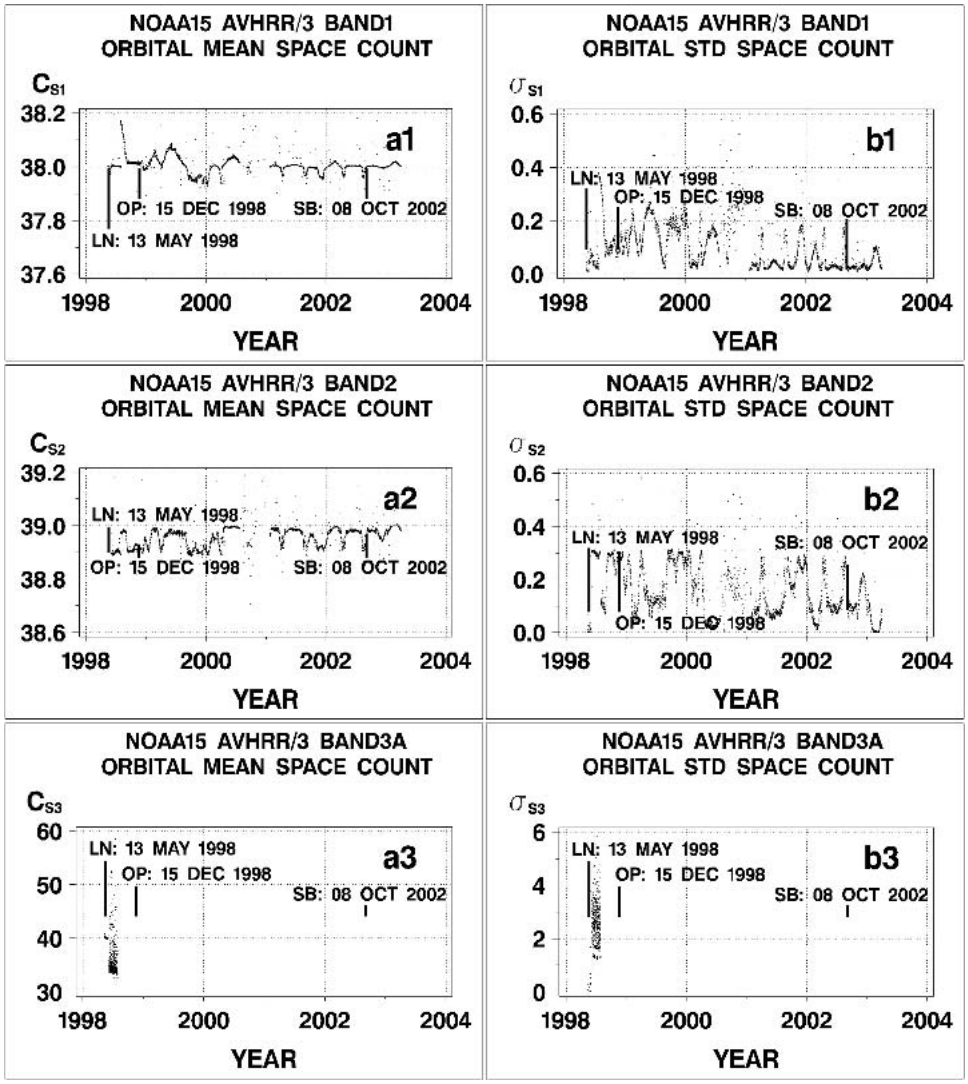

FIG. 14. Same as in Fig. 12, but for AVHRR/3 on board *NOAA-15*. (bottom) Band 3A was discontinued shortly after launch, before *NOAA-15* became operational.

bands 1 and 2 is lower compared to the prelaunch estimates. Its high variability in time may result from frequent Moon events and from the fact that this platforms flies near the terminator, and thus may additionally experience contamination from the Sun. Not much effort was invested in calibrating its SRBs in-flight, as they are of little use on the morning *NOAA-15*, which flies in half-dark all the time. Note that the band 3A on *NOAA-15* was discontinued shortly after launch, in favor of the 3B band at 3.7 μm.

The two most recent KLM afternoon platforms, *NOAA-16* and *-17*, are used, among other applications, for the operational retrievals of aerosol over oceans (Ignatov et al. 2004) and a vegetation index over land. Performance of their AVHRR/3 SRBs is critical for the quality of these products. Time series of the respective SCs are plotted in Figs. 15–16 and show more regular (less noisy) behavior compared to *NOAA-15*. On *NOAA-16*, the SC varies within 0.2–0.3 counts in all three bands. The STDs are from 0.2–0.5 counts in bands 1 and 2, and ~1.3 counts in band 3A, consistently higher compared to their prelaunch estimates in Table 1b. For *NOAA-17*, the trends are a few tenths of a count in less than a year. The noise in bands 1 and 2 is ~0.6 counts and 0.75 counts in band 3A, again higher compared to their prelaunch estimates, but lower compared to *NOAA-16*. (Recall that assuming all other things being equal, the amplitudes of time trends, and STD values for AVHRR/3 are expected to be a factor of ~2 to ~4 larger compared to AVHRR/1 and /2, in count units, simply due to improved digitization in its low gain.)

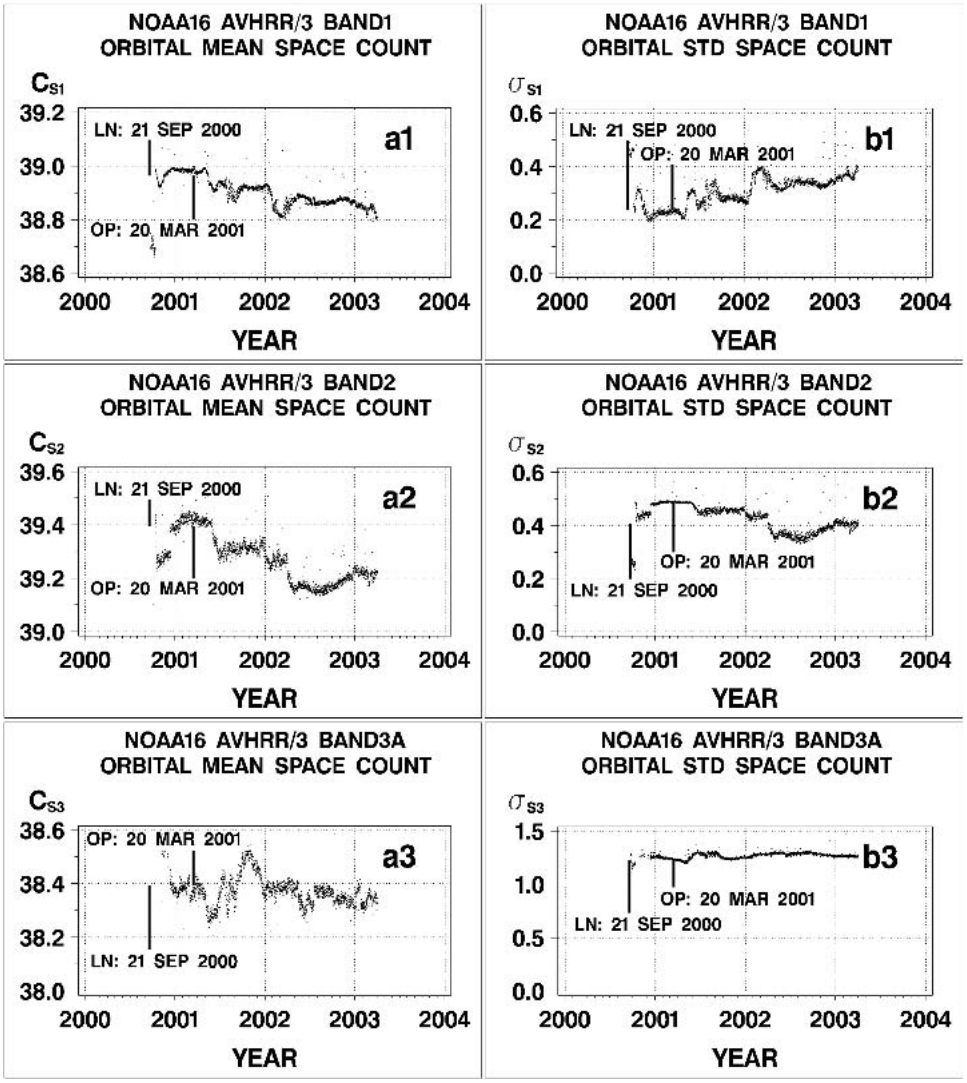

FIG. 15. Same as in Fig. 14, but for AVHRR/3 on board *NOAA-16*. Band 3A was discontinued on 1 May 2003.

c. *The use of the SC statistics to define the ZC in the long-term AVHRR reprocessing*

Visual inspection of the SC variability in Figs. 10a–16a, in conjunction with the sensitivity estimates in section 2c, clearly suggests that in-flight SC data should be used to specify the ZC in the long-term AVHRR processing. Two aerosol climate data records (CDRs) have been produced so far: PATMOS (from *NOAA-7*, *-9*, *-11*, and *-14*; Stowe et al. 2002), and the Global Aerosol Climatology Project (GACP) based on the International Satellite Cloud Climatology Project (ISCCP; Mishchenko et al. 2003). Equation (3) was used to calibrate the AVHRR/2 SRBs for the PATMOS dataset. The values of ZC were set at $C_{o1} \sim 36.0$, $C_{o2} \sim 37.0$ for *NOAA-7*; $C_{o1} \sim 37.0$, $C_{o2} \sim 39.6$ for *NOAA-9*; $C_{o1} \sim 40.0$, $C_{o2} \sim 40.0$ for *NOAA-11*; $C_{o1} \sim 42.7$, $C_{o2} \sim 39.4$ for *NOAA-12*; and $C_{o1} \sim 41.0$, $C_{o2} \sim 41.0$ for *NOAA-14*. For all platforms, with the exception of *NOAA-14*, these numbers differ from in-flight estimates. In the GACP aerosol dataset, the ISCCP calibration was utilized. Geogdzhayev et al. (2002) and Mishchenko et al. (2003) suggest that at least a part of the residual trend in their aerosol multiyear time series originates from an unaccounted variability in the ZC parameter of Eq. (3).

The mean SC can be considered a proxy for the ZC only to a first approximation, and a better job can and should be done to estimate the ZC from the SC more accurately. A rigorous quality control is needed to remove the outliers (such as the Moon events similar to those considered in section 4), and suppress noise by averaging and temporal smoothing. One should remember that even in such case, the orbital mean and STD might not be representative of the true ZC and

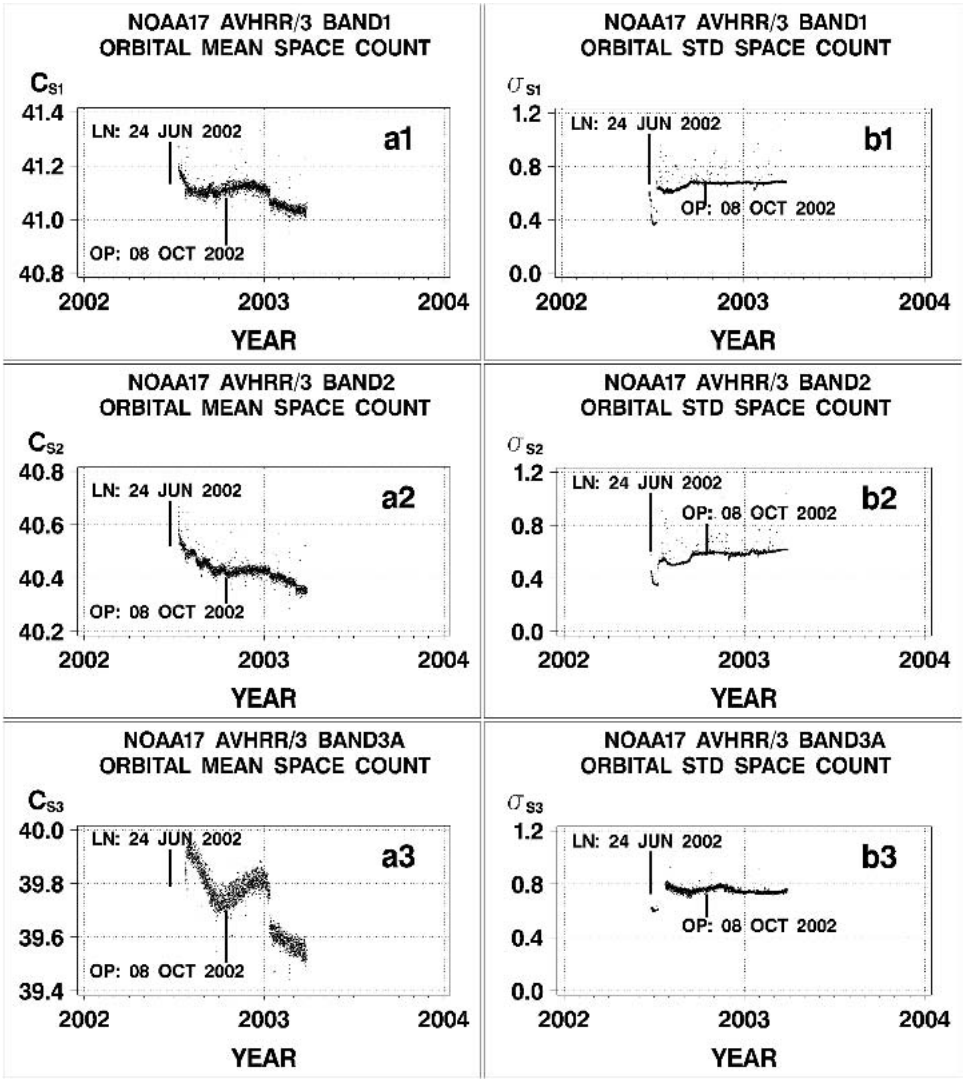

FIG. 16. Same as in Fig. 14, but for AVHRR/3 on board *NOAA-17*. As of time of this writing, data continue to be collected in band 3A on sunlit parts of Earth. (It switches to 3B automatically when the sun angle goes over $\theta_o = 90°$.)

radiometric noise, due to digitization. The error is smaller for AVHRR/3, whose count in bands 1, 2, and 3 is ~2 and ~4 times finer compared to AVHRR/2. Analyses of the available time series are instructive to assess the typical periods and magnitudes associated with the SC on-orbit variability. Retrospective SC data should be consistently reprocessed from 1978 onward and compiled for the use in the future generations of CDRs.

7. Discussion and conclusions

Our analyses suggest that the >25-yr-long NOAA practice of discarding the AVHRR space view data ought to be changed. The onboard measurements of space count in the AVHRR solar reflectance bands should be used to better understand the radiometric performance of the SRBs, and improve their calibration accuracy in-flight. This conclusion is in broad agreement with the NOAA practice of calibrating the AVHRR EEBs and imager and sounder instruments on board the geostationary satellites (Weinreb et al. 1997) and earlier AVHRR studies (Kaufman and Holben 1993; Teillet and Holben 1994; Mitchell 2001). Using the SC information to specify the "zero count" affects the AVHRR calibration directly, through an improved calibration offset in Eq. (3), and indirectly, by constraining the preflight and vicarious determinations of the calibration slope (gain). The AVHRR calibration enhancement would improve all data products generated from AVHRR, with most noticeable effect expected in those products generated from low radiances

such as aerosol retrieval (Geogdzhayev et al. 2002; Mishchenko et al. 2003; Ignatov et al. 2004).

The terms of "zero count" [a parameter in the calibration Eq. (3)] and space count (onboard measurement) are often used in the literature indiscriminately. It is felt that one should clearly distinguish between them to emphasize the fact that the SC is a measurement, and therefore it is subject to data errors. As a result, extensive quality control and preprocessing is needed to estimate the ZC parameter from the SC data (Trishchenko 2002; Weinreb et al. 1997). Note that not all data errors can be fully mitigated, even if great care is taken in the data analyses. For instance, the digitization in the SC may introduce systematic biases in the estimated ZC. More analyses are needed to better constrain this source of error.

The current NOAA system to monitor the SC in-flight on a per-orbit basis provides a solid working infrastructure. It should be continued in the future, with the five more AVHRR/3 instruments that are scheduled to fly through at least 2020, and the future NPOESS/VIIRS instrument. Additionally, the processing should be extended back in time to include the full AVHRR period from 1978 onward.

A few improvements may be recommended. First, the current system would benefit from supplementing a physical model to predict the Moon events in the AVHRR space view to identify potential problem areas. In addition, mathematical procedures should be implemented to identify and screen out bad SC data (outliers). A full log of those bad lines should be maintained and updated periodically in order to identify and exclude from analyses the respective corrupted Earth-view data. We emphasize that robust procedures to estimate the two *true* orbital ZC statistics, mean and STD, from the digitized SC data should be developed. Checking for consistency with the night counts in the solar reflectance bands is expected to provide additional perspective to the SC data, and rule out possible out-of-band secondary peaks in the spectral filter functions that may leak thermal radiation. Time series of the SC statistics and ZCs derived therefrom should be created and analyzed and quality controlled separately. Residual interorbital noise in the time series should be suppressed/reduced by additional temporal smoothing and/or running averaging.

In addition to being an indispensable source of the information on the long-term stability and radiometric performance of the AVHRR instruments, the quality-assured time series of the space and night count statistics will provide a valuable source of the calibration offset data in historical data reprocessing and climate data records such as the Pathfinder Atmosphere (PATMOS; Stowe et al. 2002), its current successor at NOAA called the AVHRR Stewardship (J. Bates and M. Goldberg 2004, personal communication), or the Global Aerosol Climatology Project (Mishchenko et al. 2003). In the real-time NOAA operations, where data from the future are not available for smoothing, the estimated calibration offset may be therefore less accurate. Short-term extrapolation of the past time series may be used as a practical solution that in any case is more accurate compared to the current practice. The current simpler on-orbit quality control procedures used with the Earth emission bands calibration data may be temporarily applied to the SC in the solar reflectance bands before a more comprehensive system is developed and implemented. Note that the currently operational trending of the blackbody count and PRT temperature data in the AVHRR Earth emission bands should be improved, and applied consistently with the proposed SC trending. These analyses are currently under way, and their results will be reported elsewhere.

The lessons learned with the AVHRR should be carefully taken into consideration with the future NPOESS/VIIRS processing. A system to monitor, trend, and quality control a full set of the VIIRS calibration parameters should be planned to commence from the onset of the mission.

Acknowledgments. We greatly acknowledge helpful discussions with M. Weinreb (retired), N. Rao (deceased), W. Rossow (NASA/GISS, USA), A. Trishchenko (CCRS, Canada), R. Mitchell (CSIRO, Australia), D. Tarpley and I. Laszlo (NOAA/NESDIS, USA). This work was funded under the NASA EOS/CERES Contract L-90987C, the Integrated Program Office VIIRS Risk Reduction activity (NOAA/NASA/DOD), NOAA Polar System Development and Implementation (PSDI), and NOAA Ocean Remote Sensing and Joint Center for data Assimilation (NOAA/NESDIS) Programs. We are thankful to Steve Mango (IPO), Mike Mignogno and Tom Schott, Al Strong, Bill Pichel and Fuzhong Weng (NOAA/NESDIS) for their support and encouragement. In-depth constructive reviews by two anonymous reviewers helped us to clarify the major points of this study. We acknowledge Edward V. Browell and Joy Duke (NASA/LaRC) for their excellent editorial work. The views, opinions, and findings contained in this report are those of the authors and should not be construed as an official National Oceanic and Atmospheric Administration or U.S. Government position, policy, or decision.

APPENDIX

List of Acronyms Used in the Paper

a. General

AVHRR	Advanced Very High Resolution Radiometer
CDR	Climate data record
ICT	Internal calibration target
NOAA	National Oceanic and Atmospheric Administration
PRT	Platinum resistance thermistor

b. Bands

EEB	Earth emission band
SRB	Solar reflectance band

c. Parameters of calibration Eqs. (1)–(3)

RC	Reference count
ZC	Zero count

d. Views/counts

BV/BC	Blackbody view/count
CV/CC	Clamp view/count
EV/EC	Earth view/count
SV/SC	Space view/count

e. AVHRR data formats

GAC	Global area coverage
LAC	Local area coverage

REFERENCES

Abel, P., 1990: Prelaunch calibration of the *NOAA-11* AVHRR visible and near-IR channels. *Remote Sens. Environ.,* **31,** 227–229.

Cao, C., M. Weinreb, and J. Sullivan, 2001: Solar contamination effects on the infrared channels of AVHRR. *J. Geophys. Res.,* **106,** 33 463–33 469.

Cracknell, A., 1997: *The Advanced Very High Resolution Radiometer (AVHRR).* Taylor and Francis, 534 pp.

Geogdzhayev, I., M. Mishchenko, W. Rossow, B. Cairns, and A. Lacis, 2002: Global two-channel AVHRR retrievals of aerosol properties over the ocean for the period of *NOAA-9* observations and preliminary retrievals using *NOAA-7* and *NOAA-11* data. *J. Atmos. Sci.,* **59,** 262–278.

Goodrum, G., K. Kidwell, and W. Winston, Eds., 2003: NOAA-KLM user's guide. U.S. Dept. Of Commerce, NOAA/NESDIS, 522 pp. [Available from National Climatic Data Center, 151 Patton Ave, Rm. 120, Asheville, NC 28801-5001 and online at http://www2.ncdc.noaa.gov/docs/klm/index.htm.]

Ignatov, A., 2002: Sensitivity and information content of aerosol retrievals from AVHRR: Radiometric factors. *Appl. Opt.,* **41,** 991–1011.

——, 2003: Spurious signals in TRMM/VIRS reflectance channels and their effect on aerosol retrievals. *J. Atmos. Oceanic Technol.,* **20,** 1120–1137.

——, J. Sapper, S. Cox, I. Laszlo, N. R. Nalli, and K. B. Kidwell, 2004: Operational aerosol observations (AEROBS) from AVHRR/3 on board NOAA-KLM satellites. *J. Atmos. Oceanic Technol.,* **21,** 3–26.

ITT, 1997: Advanced very high resolution radiometer/3, instruction manual and alignment/calibration handbook (S/N A302). Contract NAS5-30384, ITT Aerospace/Communications Division, Fort Wayne, IN, 411 pp.

——, 1999: Advanced very high resolution radiometer/3, instruction manual and alignment/calibration handbook (S/N A301). Contract NAS5-30384, ITT Aerospace/Communications Division, Fort Wayne, IN, 406 pp.

——, 2002: Advanced very high resolution radiometer/3, instruction manual and alignment/calibration handbook (S/N A304). Contract NAS5-30384, ITT Aerospace/Communications Division, Fort Wayne, IN, 414 pp.

Kaufman, Y., and B. Holben, 1993: Calibration of the AVHRR visible and near-IR bands by atmospheric scattering, ocean glint and desert reflection. *Int. J. Remote Sens.,* **14,** 21–52.

Kidwell, K., Ed., 2000: NOAA polar orbiter data user's guide. U.S. Dept. of Commerce, NOAA, National Environmental Satellite Data and Information Service, 394 pp. [Available from National Climatic Data Center, 151 Patton Ave., Rm. 120, Asheville, NC 28801-5001 and online at http://www2.ncdc.noaa.gov/docs/podug/index.htm.]

Kigawa, S., and T. Mo, 2002: An algorithm for correction of lunar contamination in AMSU-A data. NOAA Tech. Rep. NESDIS 111, 30 pp.

Minnis, P., L. Nguyen, D. Doelling, D. Young, W. Miller, and D. Kratz, 2002: Rapid calibration of operational and research meteorological satellite imagers. I. Evaluation of research satellite visible channels as references. *J. Atmos. Oceanic Technol.,* **19,** 1233–1249.

Mishchenko, M., and Coauthors, 2003: Aerosol retrievals from AVHRR radiances: Effects of particle nonsphericity and absorption and an updated long-term climatology of aerosol properties. *J. Quant. Spectrosc. Radiat. Transfer,* **79–80,** 953–972.

Mitchell, R., 1996: Preflight calibration anomaly in the *NOAA-14* AVHRR channels 1 and 2. *Remote Sens. Environ.,* **56,** 141–147.

——, 2001: In-flight characteristics of the space count of NOAA AVHRR channels 1 and 2. CSIRO Atmospheric Research Tech. Paper 52, 24 pp.

Rao, N., and J. Chen, 1995: Inter-satellite calibration linkages for the visible and near-infrared channels of AVHRR on the *NOAA-7, -9,* and *-11* spacecraft. *Int. J. Remote Sens.,* **16,** 1931–1942.

——, and ——, 1999: Revised post-launch calibration of the visible and near-infrared channels of AVHRR on the *NOAA-14* spacecraft. *Int. J. Remote Sens.,* **20,** 3485–3491.

Stowe, L., H. Jacobowitz, G. Ohring, K. Knapp, and N. Nalli, 2002: The AVHRR Pathfinder Atmosphere (PATMOS) climate data set: Initial analyses and evaluations. *J. Climate,* **15,** 1243–1260.

Sullivan, J., 1999: New radiance-based method for AVHRR thermal channel nonlinearity correction. *Int. J. Remote Sens.,* **20,** 3493–3501.

Tahnk, W. R., and J. A. Coakley, 2002: Improved calibration coefficients for *NOAA-12* and *NOAA-15* AVHRR visible and near-IR channels. *J. Atmos. Oceanic Technol.,* **19,** 1826–1833.

Teillet, P., and B. Holben, 1994: Towards operational radiometric calibration of NOAA AVHRR imagery in the visible and near-IR channels. *Can. J. Remote Sens.,* **20,** 1–10.

Trishchenko, A., 2002: Removing unwanted fluctuations in the AVHRR thermal calibration data using robust techniques. *J. Atmos. Oceanic Technol.,* **19,** 1939–1954.

——, and Z. Li, 2001: A method for the correction of AVHRR onboard IR calibration in the event of short-term radiative contamination. *Int. J. Remote Sens.,* **22,** 3619–3624.

——, G. Fedosejevs, Z. Li, and J. Cihlar, 2002: Trends and uncertainties in thermal calibration of AVHRR radiometers onboard *NOAA-9* to *NOAA-16*. *J. Geophys. Res.,* **107,** 4778, doi:10.1029/2002JD002353.

Weinreb, M., M. Jamiesen, N. Fulton, Y. Chen, J. X. Johnson, J. Bremer, C. Smith, and J. Baucom, 1997: Operational calibration of *GOES-8* and *-9* imagers and sounders. *Appl. Opt.,* **36,** 6895–6904.